Rapid, low-cost detection of Zika virus using programmable biomolecular components

Authors
Keith Pardee[a*], Alexander A. Green[b*], Melissa K. Takahashi[c*], Dana Braff[c,d,e*], Guillaume Lambert[e,f*] Jeong Wook Lee[e], Tom Ferrante[e], Duo Ma[b], Nina Donghia[e], Melina Fan[g], Nichole M. Daringer[c], Irene Bosch[c], Dawn M. Dudley[h], David H. O'Connor[h], Lee Gehrke[c,i,j], and James J. Collins[c,e,j,k,l,m]

Affiliations:
[a]Leslie Dan Faculty of Pharmacy, University of Toronto, Toronto, ON, M5S 3M2, Canada; [b]Biodesign Center for Molecular Design and Biomimetics, The Biodesign Institute and the School of Molecular Sciences, Arizona State University, AZ 85287, USA; [c]Institute for Medical Engineering & Science, Massachusetts Institute of Technology, Cambridge, MA 02139, USA; [d]Department of Biomedical Engineering, Boston University, Boston, MA 02215, USA; [e]Wyss Institute for Biologically Inspired Engineering, Harvard University, Boston, MA 02115, USA; [f]School of Applied and Engineering Physics, Cornell University, Ithaca NY 14853, USA; [g]Addgene, Cambridge, MA 02139, USA; [h]Wisconsin National Primate Research Center and Department of Pathology and Laboratory Medicine, UW-Madison, Madison, WI 53706, USA; [i]Department of Microbiology and Immunobiology, Harvard Medical School, Boston, MA 02115, USA; [j]Harvard-MIT Program in Health Sciences and Technology, Cambridge, MA 02139, USA; [k]Department of Biological Engineering, Massachusetts Institute of Technology, Cambridge, MA 02139, USA; [l]Synthetic Biology Center, Massachusetts Institute of Technology, Cambridge, MA 02139, USA; [m]Broad Institute of MIT and Harvard, Cambridge, MA 02142, USA.
* co-first authors

Contact information: Email: jimjc@mit.edu

Summary
The recent Zika virus outbreak highlights the need for low-cost diagnostics that can be rapidly developed for distribution and use in pandemic regions. Here, we report a pipeline for the rapid design, assembly and validation of cell-free, paper-based sensors for the detection of the Zika virus RNA genome. By linking isothermal RNA amplification to toehold switch RNA sensors, we detect clinically relevant concentrations of Zika virus sequences and demonstrate specificity against closely related Dengue virus sequences. When coupled with a novel CRISPR/Cas9-based module, our sensors can discriminate between viral strains with single-base resolution. We successfully demonstrate a simple, field-ready sample-processing workflow and detect Zika virus from the plasma of a viremic macaque. Our freeze-dried biomolecular platform resolves important practical limitations to the deployment of molecular diagnostics in the field, and demonstrates how synthetic biology can be used to develop diagnostic tools for confronting global health crises.

Introduction

The emerging outbreak of Zika virus in the Americas has brought this once obscure pathogen to the forefront of global healthcare. Mostly transmitted by *Aedes aegypti* and *A. albopictus* mosquitoes, Zika virus infections have been further spread by international travel, and have expanded to large, heavily populated regions of South, Central and North America (Bogoch et al., 2016). Correlations between the increase in Zika virus infections and the development of fetal microcephaly (Calvet et al., 2016; Galindo-Fraga et al., 2015; Victora et al., 2016) and Guillain–Barré syndrome have resulted in the declaration of a public health emergency by the World Health Organization (WHO) and a call for fast-tracked development of Zika virus diagnostics (Oehler et al., 2014; Smith and Mackenzie, 2016; WHO, 2016).

Synthetic biology is an emerging discipline that has great potential to respond to such pandemics. The increasing ability of synthetic biologists to repurpose and engineer natural biological components for practical applications has led to new opportunities for molecular diagnostics (Kotula et al., 2014; Lu et al., 2013; Slomovic et al., 2015). We previously developed two biotechnologies that dramatically lower the cost of and technical barriers to the development of synthetic biology-based diagnostics. The first

technology, programmable RNA sensors called toehold switches, can be rationally designed to bind and sense virtually any RNA sequence (Green et al., 2014). The second technology, a freeze-dried, paper-based, cell-free protein expression platform, allows for the deployment of these toehold switch sensors outside of a research laboratory by providing a sterile and abiotic method for the storage and distribution of genetic circuits at room temperature (Pardee et al., 2014). We combined these technologies to create a platform for rapidly and inexpensively developing and deploying diagnostic sensors.

In the context of the Zika virus outbreak, the paper-based sensors offer a solution to the critical challenges facing diagnosis of the virus. Standard serological approaches, such as antibody detection, are limited in diagnostic value due to cross-reactivity in patients that have previously been infected by other flaviviruses circulating in the region. As a result, accurate diagnosis requires nucleic acid-based detection methods, such as PCR and isothermal nucleic acid amplification (Lanciotti et al., 2008; de M Campos et al., 2016; Tappe et al., 2014; Zammarchi et al., 2015). However, such techniques are relatively expensive, require technical expertise to run and interpret, and utilize equipment that is incompatible with use in remote and low-resource locations where surveillance and containment are critically needed.

Here, we demonstrate the rapid development of a diagnostic workflow for sequence-specific detection of Zika virus that can be employed in low-resource settings (Figure 1). We have addressed limitations in the practical deployment of nucleic acid-based molecular diagnostics by combining isothermal RNA amplification with toehold switch sensors on our freeze-dried, paper-based platform. We automate the amplification primer and sensor design process using *in silico* algorithms and demonstrate a high-throughput pipeline to assemble and test 48 Zika sensors in less than seven hours. Clinically relevant sensitivity is attained using our amplification and detection scheme, and we report no significant detection of the closely related Dengue virus. To further increase diagnostic capabilities, we develop a CRISPR/Cas9-based module that discriminates between Zika genotypes with single-base resolution. Finally, we employ a simple sample-preparation protocol to reliably extract viral RNA, and demonstrate robust detection with this scheme using active Zika virus samples.

Results

In silico toehold switch design

Toehold switch sensors are programmable synthetic riboregulators that control the translation of a gene via the binding of a *trans*-acting trigger RNA. The switches contain a hairpin structure that blocks gene translation in *cis* by sequestration of the ribosome binding site (RBS) and start codon. Upon a switch binding to a complementary trigger RNA, sequestration of the RBS and start codon is relieved, activating gene translation (Figure 2A and 2B) (Green et al., 2014). To allow for colorimetric detection of trigger RNA sequences, the sensors can be designed to regulate translation of the enzyme LacZ, which mediates a color change by converting a yellow substrate (chlorophenol red-β-D-galactopyranoside) to a purple product (chlorophenol red).

Toehold switch sensors for sequence-based detection of Zika virus were generated using a modified version of the previously developed *in silico* design algorithm (Supplemental Information) (Green et al., 2014). The modified algorithm screened the genome of the Zika strain prevalent in the Americas (Genbank accession number: KU312312) for regions compatible with RNA amplification and toehold switch activation. The selected Zika genome regions were then computationally filtered to eliminate potential homology to the human transcriptome and to a panel of related viruses, including Dengue and Chikungunya. A total of 24 unique regions of the Zika genome compatible with downstream sensing efforts were identified.

Two toehold switches, each utilizing a different design scheme, were designed for each region, resulting in a total of 48 sensors. The first design scheme, termed the A series, utilizes a modification to the original toehold switch (Green et al., 2014) that reduces the size of the loop domain from 18-nts to 11-nts

(Figure 2A) to discourage loop-mediated docking of the ribosome and therefore reduce leakage in the OFF state. The second design scheme, termed the B series, features a 12-nt loop and incorporates a more thermodynamically stable stem in order to lower OFF state gene expression (Figure 2B).

Rapid, in vitro sensor assembly and screening

In vitro assembly and initial screening of all 48 sensors took place in a seven-hour time period, with low costs associated with sensor development (DNA input $20 USD/sensor) and testing ($0.10 - $1/test). All 48 sensors and 24 targeted genomic regions were assembled in-house using *in vitro* protocols. Toehold switches were constructed by ligating the sensors (~130 nt) to a LacZ reporter element in a single two-hour PCR-based step. Sensor performance screening to assess each sensor against its respective trigger RNA element (Zika genome fragment) was completed using low volume, cell-free transcription and translation reactions on paper. We found that 25 (52%) of the 48 sensors produce a fold change of five or greater in the presence of the appropriate trigger element (128 - 178 nucleotide regions of the Zika genome; Figures 2C, 2D and S1). The top-ranked sensors exhibited activation as high as 34-fold over sensor alone (sensor 27B), and were activated in as quickly as 20 minutes after incubation at 37°C (sensors 7A and 8A). For all sensors, maximum fold change occurred within the first 90 minutes. Averaging the LacZ output from sensors not exposed to trigger RNA confirmed that the low background design of the series B toehold switch sensors successfully reduced signal leakage (Figure 2D inset).

Assessing and improving Zika sensor sensitivity

We selected top performing sensors from both the A and B series for trigger RNA titration experiments, and found that all chosen sensors were activated with as little as 30 nM of trigger RNA (Figure 3A). The sensors displayed a linear response to RNA concentration, providing semi-quantitative information on input trigger RNA values (Figure S2A). Additionally, our top three sensors were highly orthogonal to each other when challenged with a high dose of trigger RNA from off-target Zika sequences (3000 nM) (Figure S2B).

Though the sensors displayed specificity for their respective Zika RNA trigger, they were unable to detect clinically relevant RNA concentrations. Zika viral loads have been documented as high as 202×10^6 copies/ml (365 fM) in urine (Gourinat et al., 2015). However, viral loads in saliva and serum are reportedly even lower, with 3×10^6 copies/ml (4.9 fM) (Barzon et al., 2016) documented in patient saliva and 2.5×10^6 copies/ml (4.1 fM) (Zika experimental science team) and 7.2×10^5 copies/ml (1.2 fM) (Lanciotti et al., 2008) in primate and patient serum respectively. Accordingly, to increase the sensitivity of our diagnostic platform, we incorporated an isothermal RNA amplification technique known as NASBA (nucleic acid sequence-based amplification) into our workflow (Figure 1).

NASBA is a promising candidate for use with our diagnostic scheme because it is known to be extremely sensitive and has a proven track record in field-based diagnostic applications (Cordray and Richards-Kortum, 2012). The amplification process begins with reverse transcription of a target RNA that is mediated by a sequence-specific reverse primer to create an RNA/DNA duplex. RNase H then degrades the RNA template, allowing a forward primer containing the T7 promoter to bind and initiate elongation of the complementary strand, generating a double-stranded DNA product. T7-mediated transcription of the DNA template then creates copies of the target RNA sequence. Importantly, each new target RNA can be detected by the toehold switch sensors and also serve as starting material for further amplification cycles. NASBA requires an initial heating step (65°C), followed by isothermal amplification at 41°C (Figure 3B) (Guatelli et al., 1990).

NASBA was performed on trigger RNA corresponding to Zika genomic regions for sensors 27B and 32B. Trigger RNAs were spiked into either water or human serum (7%) to more closely mimic clinical samples. NASBA reactions were run for two hours and then applied to freeze-dried, paper-based sensors. We saw detection with Zika sensors from NASBA reactions initiated with as little as 3 fM of trigger RNA

(Figure 3C), a value within the range of reported patient viral loads. Zika sensor detection of NASBA-amplified trigger RNA proved to be reliable on samples spiked into either serum or water (Figure S2C). Additionally, for reactions initialized with high concentrations of trigger RNA (>300 fM), NASBA reaction times could be reduced to as little as 30 minutes (Figure S2D). NASBA reagents are compatible with freeze-drying (Figure S2E) and could therefore be easily deployed and utilized alongside our paper-based sensors. We also demonstrated that NASBA can be run in the absence of the initial heating step (65°C) (Figure S2F), further reducing the technical and power requirements for deployment.

Moving toward a field-ready diagnostic platform

To move our experiments toward conditions more representative of those found in clinics worldwide, we focused on three key efforts: (1) testing sensor specificity against related viruses that share clinical symptoms, partial homology, and geographic range with Zika virus, (2) building a second-generation portable, battery-powered reader to provide lab-quality results in low-resource environments, and (3) developing a low-cost and tractable method for viral RNA extraction.

Although our sensor design algorithm screened for Zika genomic sequences that are mostly distinct from those of related viruses, the targeted Zika sequences do share substantial similarity (51%-59%) with their Dengue virus counterparts (Figure S3A and S3B). To test the Zika sensors for possible cross-reactivity, we exposed the sensors to regions of the Dengue genome that share a degree of homology with regions targeted in the Zika genome. Sensors 27B and 32B were treated with high concentrations of RNA amplicons (3000 nM) from either Zika or Dengue genomic regions. As seen in Figure 4A, Dengue RNA sequences failed to activate the toehold switch sensors. We also tested our NASBA primer sets for specificity to their targeted Zika sequences by applying the NASBA-mediated amplification and paper-based detection scheme to 300 fM inputs of the Dengue and Zika RNA in human serum (7%). Again, we did not see a response to the Dengue RNA sequences, demonstrating robust sequence specificity in our amplification and detection scheme (Figure 4B).

As part of our efforts to advance the paper-based sensor platform toward field-ready diagnostics, we designed a second-generation portable electronic reader to serve as an accessible, low-cost companion technology that provides robust and quantitative measurements of sensor outputs. The electronic reader was assembled using readily available consumer components, open-source code, and laser-cut acrylic housing, with a total cost of just under $250 (Figure S4 and Table S3). The reader is powered by a lithium ion battery (18.5 hours) that can be re-charged via micro USB, and houses onboard data storage (4 GB) to resolve the need for an attached laptop during diagnostic reads (Pardee et al., 2014). To achieve sensitive detection of toehold switch signal output, an acrylic chip that holds the freeze-dried, paper-based reactions is placed into the reader between an LED light source (570 nm) and electronic sensors (Figure S4B). Using onboard electronics, each sample is read 29 times per minute, providing low-noise measurements of changes in light transmission due to LacZ-mediated color change.

To demonstrate the utility of the companion reader, we monitored detection of 1 fM and 3 fM of Zika RNA amplicons that had been amplified in NASBA reactions for 2.5 hours. The reader detected significant signal from both samples, which are within the reported range of Zika virus in patient serum (1.2 fM) and urine (365 fM) (Gourinat et al., 2015; Lanciotti et al., 2008), after just over 20 minutes (Figure 4C).

Our next challenge was to develop a technique to release RNA from the viral capsid using simple methodology compatible with low-resource environments. To this end, we tested the efficacy of boiling viral samples to break down the capsid. For initial development, we engineered lentivirus, which is also an RNA virus, to encapsulate the regions of either the Zika or Dengue genomes that correspond to the sensor 32B target sequence (Figure S3B). These proxy Zika and Dengue viruses were spiked into human serum (7%) at a final concentration of 3 fM, and heated to 95°C for either one or two minutes. The

resulting lysates were then immediately used to initiate NASBA reactions, in order to simulate what might be recovered from a patient sample. Boiling the viral samples for one minute was sufficient to release detectable amounts of RNA in our amplification and toehold switch detection scheme (Figure S3C). NASBA reactions from two-minute boiled samples were also monitored for sensor activation on the portable electronic reader. We detected strong sensor activation in less than 30 minutes from 3 fM of lentivirus carrying Zika RNA. We were also able to demonstrate clear discrimination between lentiviruses containing Zika and Dengue RNA sequences (Figure 4D).

A NASBA-CRISPR cleavage assay to discriminate between Zika strains

During epidemic outbreaks, it is often valuable to monitor pathogen lineage and geographic spread. In some cases, genetic variants may be responsible for different clinical manifestations of infection. For example, the Zika strain found in Brazil has been uniquely connected with higher incidences of fetal microcephaly and Guillain-Barre syndrome (Calvet et al., 2016; Mlakar et al., 2016). To allow for strain-specific detection and tracking, we developed an assay that provides single-base discrimination in a manner that is compatible with our freeze-dried sensor platform. Our assay, which we term NASBA-CRISPR Cleavage (NASBACC), leverages the sequence-specific nuclease activity of CRISPR/Cas9 to discriminate between viral lineages (Figure 5A). To do this, NASBACC exploits the ability of Cas9 to selectively cleave DNA only in the presence of an NGG protospacer adjacent motif (PAM). Since any non-biased mutation has a 48% probability of either creating a new PAM site or destroying an existing one (Table S4), there are many strain-specific PAM sites that can be used for lineage discrimination (Figure 5B and 5C). In the NASBACC detection scheme, RNA sequences undergo NASBA amplification utilizing a reverse primer designed to append the trigger sequence of a synthetic toehold switch (sensor H, Figure 5A) (Pardee et al., 2014). In the presence of the appropriate PAM sequence and guide RNA target site, the double-stranded DNA that is synthesized as part of the NASBA reaction undergoes Cas9-mediated cleavage, resulting in a truncated RNA product that is unable to activate the sensor H toehold switch. In the absence of the PAM sequence, the full-length RNA product containing the sensor H trigger sequence is generated, allowing for sensor H activation. Trigger RNA is only amplified from DNA that is not cut by Cas9, thereby allowing for strain-specific detection using toehold sensor H.

Using the paper-based system, sensor 32B was able to distinguish between Zika and Dengue RNA sequences. However, this sensor could not discriminate between the African (Genbank accession number: KF268950) and American (Genbank accession number: KU312312) Zika variants (Figure 5D), a feature which may be useful in certain diagnostic applications. To address this, we applied our NASBACC detection scheme to discriminate between the African and American Zika strains. Due to a single-base difference in the trigger regions of these two strains, a PAM site only exists in the American-lineage sequence (Figure 5C). Thus, only the American strain sequence was cleaved by Cas9, which led to amplification of truncated RNA that did not activate the sensor H toehold switch (Figure 5E). Conversely, the African strain sequence does not contain the PAM site and was not cleaved by Cas9, which resulted in amplification of full-length RNA that activated the sensor H toehold switch. Incorporating NASBACC into our diagnostic workflow can provide precise genotypic information within a few hours. As with the other biomolecular elements of this workflow, Cas9 is compatible with lyophilization and could be used in the field (Figure S5).

Diagnostic workflow validation with active Zika virus

We next sought to validate our sensor platform with live Zika virus. First, we verified that our amplification and detection scheme could successfully detect full-length genomic RNA purified from Zika virus (Uganda strain MR 766) (Figure 6A). We designed new NASBA primers to accommodate sequence differences between the Uganda Zika strain (Genbank accession number: AY632535) and the American Zika strain (Genbank accession number: KU312312) that our sensors and primers had originally been designed to detect. Computational analysis suggested that Uganda-lineage Zika RNA would activate sensor 32B despite two base mismatches in the toehold region, and this was confirmed

experimentally (Figure 6A). We also demonstrated sensor orthogonality to full-length genomic Dengue RNA isolated from three different Dengue serotypes using these methods (Figure 6A).

Once we confirmed that the sensors behaved as expected on full-length genomic RNA, we sought to validate the sample preparation scheme and diagnostic workflow from start to finish. Active Zika virus was cultured in the laboratory and spiked into human serum (7%) at a final concentration of 10 fM, to mimic a clinical sample. The viral sample was then heated to 95°C for two minutes, and the resulting lysate was subjected to NASBA amplification for three hours. Sensor activation from the NASBA-amplified viral sample was monitored on the portable electronic reader. We successfully detected activation of sensor 32B from a diagnostic workflow initiated with live Zika virus (Figure 6B).

For the final validation of our system, we acquired and tested plasma samples from a viremic macaque infected with Zika virus (Genbank accession number: KJ776791) (Zika experimental science team). The macaque was found to have a plasma viral load of 1.7×10^6 copies/ml (2.8 fM) by a standard qRT-PCR protocol, which was within the detection limits of our platform as tested on synthetic RNA amplicons (Figure 4C). The viremic plasma was diluted 1:10 in water to reduce known inhibitory effects of plasma on downstream reactions, and was then taken through our sample processing and diagnostic workflow. The sample was heated to 95°C for two minutes and then amplified via NASBA for three hours. Paper-based reactions were monitored on the portable electronic reader, and showed strong activation with both sensors 27B and 32B in less than 30 minutes (Figure 6C and 6D).

Discussion

Rapid sensor development pipeline for low-resource molecular diagnostics

We have devised a rapid diagnostic development pipeline in response to the ongoing Zika virus outbreak. The serious but poorly understood complications of this viral infection make its timely diagnosis critical for patient health and for limiting its rapid proliferation. However, the poor performance of antibody detection methods (Lanciotti et al., 2008; de M Campos et al., 2016; Tappe et al., 2014; Zammarchi et al., 2015) and the limitations of traditional sequence-based diagnostics have left technical and economic challenges to meeting diagnostic needs.

Our paper-based platform directly addresses these needs by enabling sequence-specific detection of Zika virus in a low-cost manner that is tractable in low-resource settings. By freeze-drying cell-free transcription and translation systems with genetic sensors onto paper, we have created a sterile and abiotic platform that can be utilized outside of laboratory conditions without concern over biosafety. Furthermore, the freeze-dried biomolecular components remain stable at room temperature, allowing for easy storage and distribution in global settings. Our application is easy to use, relying on a colorimetric output that can be read by the naked eye or with a low-cost, battery-operated companion reader, and we are actively working to improve field-readiness via development of a third-generation reader with onboard capabilities for sample preparation and incubation.

The streamlined sensor development platform we describe here provides a generalizable method for a rapid response to any emerging outbreak. Our automated design process computationally screens for sequence specificity and feeds into a high-throughput protocol for rapid sensor prototyping *in vitro*. We augmented our diagnostic sensors with an upstream target-amplification scheme that allows for detection of target sequences in the low femtomolar range, bringing sensor sensitivity in line with in-patient virus concentrations (Gourinat et al., 2015; Lanciotti et al., 2008). Additionally, we demonstrated that simply boiling an RNA virus liberates sufficient material for downstream amplification and detection processes (Figures 4D, 6 and S3C), and we developed a CRISPR-based tool for accurate strain genotyping on paper (Figure 5). Finally, our methods were validated on viremic plasma samples (Figure 6C and 6D), demonstrating a level of sensitivity that would be required for use of this diagnostic scheme in the field.

Isothermal RNA amplification and nucleic acid-based diagnostics for low-resource settings
Our unique approach of linking NASBA to a downstream synthetic gene network for output detection can be applied to any nucleic acid amplification scheme. This innovative development addresses several key technical and economic challenges in the employment of isothermal amplification methods in the field. Namely, although NASBA has exceptional sensitivity to low-level infections, the technique is costly ($5-$20/test) and susceptible to contamination that can lead to off-target products and false positives (Casper et al., 2007; Cordray and Richards-Kortum, 2012; Ulrich et al., 2010). Our diagnostic scheme addresses both of these points and brings NASBA closer towards application in low-resource settings. The low volume paper-based reactions only use a fraction of a microliter of NASBA product ($0.51/μl), significantly reducing the total cost of NASBA per test. Additionally, linking NASBA to a synthetic gene network for signal detection allows for rapid and sensitive output reads in a cost-effective manner ($0.10 - $1/test) that is practical for use in low-resource settings. Furthermore, the chance for false positive results due to contamination is minimized by the use of sequence-specific toehold switch sensors and CRISPR/Cas9-mediated selection downstream of the amplification. Our ability to eliminate the initial 65°C heating step (Figure S2F) traditionally used in NASBA reactions streamlines the diagnostic protocol for in-field use and reduces the requirements of the hardware necessary for monitoring results. Finally, we have shown that NASBA reagents can be freeze-dried (Figure S2E) and therefore could be distributed around the world at room temperature alongside our toehold switch sensors. We are also actively working towards combining NASBA and toehold switch sensor reactions in a one-pot assay that will further streamline the diagnostic protocol and shorten the timeframe for readout.

We note that certain components within blood are known to inhibit PCR (Schrader et al., 2012) and similarly affect all nucleic acid based diagnostics, including NASBA. However, we found that a simple dilution of serum or plasma into water sufficiently removes this effect in our diagnostic scheme. We therefore used diluted human serum (7%) as a matrix for our exploratory experiments, and diluted viremic plasma samples (10%) for our final validation experiment. The dilution step does affect the overall sensitivity of the diagnostic platform, but we have shown that increasing the NASBA reaction time can sufficiently compensate for reduced sensitivity. Indeed, we were able to detect 2.8 fM of Zika virus from plasma samples from an infected rhesus macaque using our dilution protocol (Figure 6C and 6D). Additionally, a recent study found that Zika virus can be detected at high concentrations in saliva (Barzon et al., 2016), which may not inhibit nucleic acid amplification to the same extent as blood. We are actively working to test other clinical matrices for compatibility with our diagnostic platform.

A robust and field-ready sample preparation scheme for RNA viruses
In this work, we implemented a simple procedure to extract viral RNA that does not require specialized laboratory equipment. By simply boiling (95°C) virus samples for two minutes, we were able to extract sufficient quantities of RNA for amplification and detection in our diagnostic platform (Figure 4D and 6B, 6C, and 6D). We note that we worked quickly to transfer boiled viral samples to NASBA reactions that contained RNase inhibitors to protect the integrity of the viral RNA. In practice, other commercially available reagents could be added to the sample to protect the RNA from degradation upon collection. Of note, we were able to reliably extract RNA from three different sample types using our methodology: engineered lentivirus (Figure 4D), cultured Zika virus (Figure 6B) and plasma from an infected rhesus macaque (Figure 6C and 6D), highlighting the robustness of our sample preparation scheme.

Programmability of molecular sensors can address rapidly changing diagnostic needs
Our platform provides multiple levels of molecular programmability that greatly improve diagnostic specificity. Both the toehold switches and NASBA primers can be designed to target regions specific to a given genome, while excluding regions with significant homology to other organisms. We demonstrated the effectiveness of this design algorithm with sensor 32B, which was able to distinguish genomic Zika RNA from the genomic RNA of three different Dengue serotypes (Figure 6A). Additionally, the NASBACC module allows for single-base discrimination and can be rationally designed to distinguish

between different genotypes, adding to the overall programmability of our platform (Figure 5E). Given the high sensor success rate and low barriers to development, we envision that sensors could be easily multiplexed to ensure high confidence diagnosis (reducing both false negative and false positive results) while keeping costs low. Furthermore, the diagnostic platform could be deployed as panels that include sensors for strain-specific identification and related infections to help monitor the spread of illness.

However, in some cases, it is beneficial for a diagnostic platform to be able to tolerate genetic mutations within a particular nucleic acid sequence. Evolutionary drift, for example, is an unavoidable feature of our ongoing arms race with pathogens that all molecular diagnostics must confront. Our assay in particular has the capacity to tolerate the expected genetic variation found in nature. We analyzed the binding between the toehold switch 32B and RNA sequences from homologous regions in Zika strains isolated from Africa and Asia (Supplemental Information: Extended Experimental Procedures). Both of these strains are predicted to fully activate the toehold sensors, even with up to 4-nt (11%) mismatches. In fact, we were able to demonstrate this using RNA triggers from the American strain, two different African strains and an Asian-lineage of the virus (Figure 5D and 6). Additionally, a critical feature of our technology is the ability to rapidly and inexpensively prototype new genetic sensors, thus allowing for a rapid response to genetic variations and mutations as they arise.

Freeze-dried biomolecular networks for addressing real-world issues in real time

With our goal of responding to the ongoing outbreak in a timely manner, we began our work using synthetic RNA fragments spiked into human serum, followed by engineered lentiviruses to mimic clinical samples. As with many proof-of-concept diagnostic studies, synthetic samples provided us with a powerful tool for optimizing our sensor platform ahead of the regulatory demands required for use of live pathogens (Antunes et al., 2015; Crannell et al., 2014; Rohrman et al., 2012; Stefan et al., 2016; Yen et al., 2015). Through collaborative efforts with the Zika virus community, we were able to test our platform on live Zika virus, and were pleased to find similar detection thresholds with Zika virus isolated from infected Vero cells (Figure 6B) and plasma samples from an infected rhesus macaque (Figure 6C and 6D). Our rapid response to the ongoing Zika virus outbreak and our ability to achieve clinically relevant sensitivity and specificity highlight the utility and practicality of this platform technology.

Our synthetic biology pipeline for rapid sensor design and prototyping could be applied to a broad range of public health threats, allowing for rapid development of new diagnostics when and where they are most needed. The ease of *in vitro* sensor synthesis will allow for the widespread use of validated sensor sequences, aiding rapid global responses to current and future health crises. Finally, our ability to expeditiously design and implement our biomolecular diagnostics for an emerging pathogen using the engineering principles of synthetic biology suggests that the field will play an ever-increasing role in the support and improvement of human health.

Experimental Procedures

In silico sensor design and DNA synthesis

A set of 48 toehold switch sensors and corresponding NASBA primers were generated using an integrated *in silico* design algorithm. See the Extended Experimental Procedures section in the Supplemental Information for details.

DNA sensor assembly

Toehold switch constructs were amplified from DNA templates (Integrated DNA Technologies) and ligated to the *lacZ* reporter gene via PCR. Plasmids were constructed for characterization of the top six toehold switches (Figure 3A). The DNA templates were amplified using PCR and inserted into pET system parent plasmids (EMD Millipore) using Gibson assembly (Gibson et al., 2009) with 30 bp overlap regions. Plasmids for sensors 27B and 32B are available through Addgene (plasmid numbers: 75006 – 75011).

Cell-free reactions
Details of RNA sensor validation are described in Pardee et al. (2014). Briefly, amplified sensor DNA was column purified and tested on paper discs (2 mm) containing freeze-dried, cell-free reactions (NEB, PURExpress) in the presence or absence of trigger RNA coding for a complementary region of the Zika virus genome (128 – 178 nts). The cell-free reactions consisted of: NEB Solution A (40%) and B (30%), chlorophenol red-β-D-galactopyranoside (Sigma, 0.6 mg/ml), RNase inhibitor (Roche, 03335402001; 0.5%), and linear DNA constructs encoding the toehold sensors (0.33 nM). The paper discs (Whatman, 1442-042) were blocked in 5% BSA overnight prior to use. Trigger RNA was produced using T7 RNAP-based transcription (Epicentre ASF3257) from linear DNA templates. Paper-based reactions (1.8 µl) were incubated at 37°C using either our companion electronic reader inside a humidified chamber or a plate reader (BioTek Neo). For the in-house reader, paper discs were placed into 2 mm holes in a removable acrylic chip; for the plate reader, paper discs were placed into black, clear bottom 384-well plates (Corning 3544).

NASBA
For NASBA reactions, the trigger elements (128 – 178 nts) were extended by 100 nts on the 5' and 3' ends with the relevant Zika genome sequence to provide suitable template RNAs. RNA amplicons were spiked into 7% human serum (Sigma H4522) where indicated. Reaction Buffer (Life Sciences NECB-24; 33.5%), Nucleotide Mix (Life Sciences NECN-24; 16.5%), RNase inhibitor (Roche, 03335402001; 0.5%), 12.5 µM of each NASBA primer (2%), nuclease free water (2.5%), and RNA amplicon (20%) were assembled at 4°C and incubated at 65°C for 2 min, followed by a 10-min incubation at 41°C. Enzyme Mix (Life Sciences NEC-1-24; 25%) was then added to the reaction (for a final volume of 5uL), and the mixture was incubated at 41°C for 2 hours unless noted otherwise. For output reads with paper-based toeholds, the NASBA reactions were diluted 1:7 in water. See Table S2 for primer sequences.

Lentivirus preparation and processing
HEK293FT cells (Life Technologies, R70007) used for virus packaging were cultured in DMEM supplemented with 10% FBS, 1% penicillin-streptomycin, and 4 mM GlutaMAX™ (ThermoFisher Scientific). Twelve hours prior to transfection, 6.5 x 10^6 cells were seeded in a 10 cm dish. 7.5 µg psPAX2, 2.5 µg pMD2.G, and 10 µg pSB700 modified to include a Zika or Dengue RNA fragment were transfected using the HeBS-$CaCl_2$ method. Media was changed 12 hours post-transfection. Twenty-seven hours after changing media, viral supernatant was harvested and filtered using a 0.45 µm syringe filter. Viral supernatant was then purified with ViraBind Lentivirus Purification Kit (Cell Biolabs VPK-104) and buffer exchanged into 1xPBS with Lenti-X Concentrator (Clontech, 631231). Viral RNA concentration was quantified using QuickTiter Lentivirus Quantification Kit (VPK-112). Virus samples were spiked into 7% human serum at a final volume of 25 µl. Samples were heated to 95°C for 1 and 2 min and used as input to NASBA.

Zika virus preparation and processing
100 µl of Zika virus isolate (MR 766) was utilized for infection of 10^6 Vero cells in 4 ml of media (DMEM supplemented with 2% fetal calf serum (FCS) and penicillin-streptomycin). The supernatant was removed after 2 h of incubation at 37°C and replaced with fresh media (DMEM, 10% FCS) for 48 h of infection. Cell debris was removed by centrifugation at 1500 rcf for 10 minutes, and aliquots of the virus were stored at -80°C until use. The virus was buffer exchanged into 1xPBS with Lenti-X Concentrator (Clontech, 631231). Viral RNA concentrations were determined from virus purified with the QIAamp Viral RNA Mini Kit (Qiagen 52904), and confirmed with qRT-PCR. The titer of the Zika virus used was 6.7 x 10^7 infectious units per milliliter (Lambeth et al., 2005). Virus samples were spiked into 7% human serum at a final volume of 30 µl. Samples were heated to 95°C for 2 min and used as input to NASBA.

NASBA primers were re-designed to accommodate the MR 766 strain sequence (see Supplemental Information).

Dengue orthogonality
Genomic RNA from three Dengue serotypes was purified using the QIAamp Viral RNA Mini Kit (Qiagen 52904). Dengue 1 (Genbank accession number: KM204119), Dengue 2 (Genbank accession number: KM204118), Dengue 4 (Genbank accession number: AF326573). NASBA reactions using the sensor 32B primer set were performed on 30 pM RNA for 2 h. NASBA reactions were diluted 1:7 in water and used to rehydrate freeze-dried, paper-based reactions containing sensor 32B.

Electronic optical reader
The portable device consists of four layers housed within a laser-cut acrylic box fastened together with metal screws and mounting brackets (Figure S4; McMaster-Carr, 8505K14, 98164A061; Digi-Key, 36-621-ND). The top layer holds a multiplexer (Sparkfun, BOB-09056), solderable breadboard (Sparkfun, PRT-12702), friction lock connectors (Digi-Key, A31001-ND, A19473-ND) and 16 LEDs (Digi-Key, 754-1262-ND). The LEDs have a very narrow viewing angle and an emission of 570 nm to match the absorbance maximum of the chlorophenol red product from the LacZ reaction. The LEDs were placed in close proximity to the chip in the middle layer, which holds 16 paper disks within 2 mm apertures. The apertures prevented transmission of stray light and were coaxial with the LEDs in the top layer and the array of 16 TSL2591 sensors (Adafruit, 1980) in the third layer below, which also contained two solderable breadboards and connectors as above. The bottom layer contains the Arduino Uno with an attached Power Shield (Adafruit, 2708) connected to a rechargeable 2000 mAh lithium ion battery (Adafruit, 2011) on which a data-logging shield (Adafruit, 1141) was stacked with connectors (Digi-Key, A30954-ND, A19476) and a 4GB SD/MicroSD Card (Adafruit, 102). To prevent crosstalk between reads, reactions were read in series by sequentially activating each LED and sensor pair. The read frequency and pattern of the reader can be easily adjusted by modifying and uploading alternative sketches to the Arduino. The raw data (which is the median of 29 100 ms, 428x gain reads per minute) was saved to the SD card along with the date and time of the run, integration time and gain settings. The data were processed with the MATLAB script and graphed in Prism. A diagram of the circuit and an overview of the laser cut parts can be found in the supplemental figures (Figure S4) and laser cutting patterns, the Arduino sketch and MATLAB script are provided as Supplemental information files.

Calculation of fold change
The calculation of fold change for plate reader data was done by first subtracting the background absorbance measured from paper-based reactions that did not contain sensor DNA or trigger RNA. These normalized values were smoothed to reduce measurement noise using a three-point average of the time point and the data collected 10 minutes before and after. The minimum value of each well was then adjusted to zero. For data presented in Figures 3, 4 and 6, fold change was calculated from these zero adjusted values by dividing the wells at each time point by the average signal from the corresponding sensor-alone control wells. For our initial sensor screen (Figure 2), we used a more sensitive measure of fold change based on the difference in the rate of color change between control and RNA trigger wells. This was done by calculating the rate of change in normalized absorbance (570 nm) values using slope; where, at each 10 min time point, the rate was calculated using $S_n = (T_{n+1} - T_n)/10$, where T is the normalized data at a time point (T_n) and the time point 10 min later (T_{n+1}), and S_n is the slope reported for T_n. Fold change was then calculated as above.

NASBA-CRISPR Cleavage (NASBACC)
Reactions were performed in a 5 µl volume containing (NASBA buffer), 1 µl of a 250 nM Cas9 nuclease (NEB, M0386) and 250 nM purified gRNA (GeneArt precision gRNA synthesis kit, ThermoFisher Scientific, A29377) mix, 3 nM NASBACC primers, and 0.4 units of RNAse inhibitor (NEB, M0314). The forward NASBACC primer is composed of the reverse complement of the trigger H sequence (5'-

GTT TGA ATG AAT TGT AGG CTT GTT ATA GTT ATG TTT-3') and the forward binding sequence of the (region 32) NASBA primers. The reverse NASBACC primer contains the T7 promoter sequence (5'-CTA ATA CGA CTC ACT ATA GG-3') followed by the reverse binding sequence of the (region 32) NASBA primers. The assembled reaction was incubated at 37°C for 2-6 h. For toehold activation assay on freeze-dried paper, NASBACC reactions were diluted 1:10 in nuclease-free water.

Viremic plasma processing
Details on macaque care and infection can be found in the extended experimental procedures. For processing, plasma was diluted 1:10 in nuclease free water, heated to 95°C for two minutes and immediately added to a NASBA reaction. NASBA was run for three hours.

Quantitative reverse transcription PCR (qRT-PCR) to determine macaque plasma viral loads
Viral RNA was extracted from 300 µl of plasma using the Viral Total Nucleic Acid Purification Kit (Promega, Madison, WI) on a Maxwell 16 MDx instrument. Viral RNA was quantified by qRT-PCR using the primers and probe designed by Lanciotti et al. (Lanciotti et al., 2008). The RT-PCR was performed using the SuperScript III Platinum one-step quantitative RT-PCR system (Invitrogen, Carlsbad, CA) on the LightCycler 480 instrument (Roche Diagnostics, Indianapolis, IN). Primers and probe were used at final concentrations of 600 nm and 100 nm, respectively, along with 150 ng random primers (Promega, Madison, WI). Cycling conditions were as follows: 37°C for 15 min, 50°C for 30 min and 95°C for 2 min, followed by 50 cycles of 95°C for 15 s and 60°C for 1 min. Virus concentration was determined by interpolation onto an internal standard curve composed of seven 10-fold serial dilutions of a synthetic ZIKV RNA fragment based on the Asian lineage.

Author contributions
K.P. designed and performed experiments and co-wrote the manuscript. A.A.G. conceived the low-leakage toehold switches, developed the combined toehold switch and NASBA primer design algorithm, supervised sensor construction, and co-wrote the manuscript. M.K.T and D.B. designed and performed experiments and co-wrote the manuscript. G.L. developed and performed experiments for the NASBACC module and co-wrote the manuscript. J.W.L. performed the portable electronic reader experiments and edited the manuscript. T.F. designed and built the portable electronic reader and edited the manuscript. D.M. developed the rapid sensor assembly procedure and constructed sensor plasmids. N.D. performed experiments and edited the manuscript. M.F. developed the NASBA protocol. N.M.D. cultured the lentivirus samples. I.B. cultured the Zika virus samples. D.M.D. and D.H.O. provided macaque plasma samples and edited the manuscript. L.G. provided the Zika virus samples and edited the manuscript. J.J.C. designed experiments and edited the manuscript.

Acknowledgements
We would like to thank Marcelle Tuttle from the Church Lab (Wyss Institute) for the vectors used to produce the lentivirus. We would also like to thank Xiao Tan and Shimyn Slomovic for helpful comments on the manuscript, as well as Ewen Cameron, Andres Cubillos, James Niemi and Dionna Williams for assistance with project logistics. The work was supported by the Wyss Institute for Biologically Inspired Engineering, MIT's Center for Microbiome Informatics and Therapeutics, and the Defense Threat Reduction Agency grant HDTRA1-14-1-0006. A.A.G acknowledges startup funds provided by Arizona State University. L.G. acknowledges support from NIH AI100190.

References

Antunes, P., Watterson, D., Parmvi, M., Burger, R., Boisen, A., Young, P., Cooper, M.A., Hansen, M.F., Ranzoni, A., and Donolato, M. (2015). Quantification of NS1 dengue biomarker in serum via optomagnetic nanocluster detection. Sci. Rep. *5*, 16145.

Barzon, L., Pacenti, M., Berto, A., Sinigaglia, A., Franchin, E., Lavezzo, E., Brugnaro, P., and Palù, G. (2016). Isolation of infectious Zika virus from saliva and prolonged viral RNA shedding in a traveller returning from the Dominican Republic to Italy, January 2016. Euro Surveill. Bull. Eur. Sur Mal. Transm. Eur. Commun. Dis. Bull. *21*.

Bogoch, I.I., Brady, O.J., Kraemer, M.U.G., German, M., Creatore, M.I., Kulkarni, M.A., Brownstein, J.S., Mekaru, S.R., Hay, S.I., Groot, E., et al. (2016). Anticipating the international spread of Zika virus from Brazil. Lancet Lond. Engl. *387*, 335–336.

Calvet, G., Aguiar, R.S., Melo, A.S.O., Sampaio, S.A., de Filippis, I., Fabri, A., Araujo, E.S.M., de Sequeira, P.C., de Mendonça, M.C.L., de Oliveira, L., et al. (2016). Detection and sequencing of Zika virus from amniotic fluid of fetuses with microcephaly in Brazil: a case study. Lancet Infect. Dis.

Casper, E.T., Patterson, S.S., Bhanushali, P., Farmer, A., Smith, M., Fries, D.P., and Paul, J.H. (2007). A handheld NASBA analyzer for the field detection and quantification of Karenia brevis. Harmful Algae *6*, 112–118.

Cordray, M.S., and Richards-Kortum, R.R. (2012). Emerging nucleic acid-based tests for point-of-care detection of malaria. Am. J. Trop. Med. Hyg. *87*, 223–230.

Crannell, Z.A., Rohrman, B., and Richards-Kortum, R. (2014). Equipment-free incubation of recombinase polymerase amplification reactions using body heat. PloS One *9*, e112146.

Galindo-Fraga, A., Ochoa-Hein, E., Sifuentes-Osornio, J., and Ruiz-Palacios, G. (2015). Zika Virus: A New Epidemic on Our Doorstep. Rev. Investig. Clínica Organo Hosp. Enfermedades Nutr. *67*, 329–332.

Gibson, D.G., Young, L., Chuang, R.-Y., Venter, J.C., Hutchison, C.A., and Smith, H.O. (2009). Enzymatic assembly of DNA molecules up to several hundred kilobases. Nat. Methods *6*, 343–345.

Gourinat, A.-C., O'Connor, O., Calvez, E., Goarant, C., and Dupont-Rouzeyrol, M. (2015). Detection of Zika virus in urine. Emerg. Infect. Dis. *21*, 84–86.

Green, A.A., Silver, P.A., Collins, J.J., and Yin, P. (2014). Toehold switches: de-novo-designed regulators of gene expression. Cell *159*, 925–939.

Guatelli, J.C., Whitfield, K.M., Kwoh, D.Y., Barringer, K.J., Richman, D.D., and Gingeras, T.R. (1990). Isothermal, in vitro amplification of nucleic acids by a multienzyme reaction modeled after retroviral replication. Proc. Natl. Acad. Sci. U. S. A. *87*, 1874–1878.

Kotula, J.W., Kerns, S.J., Shaket, L.A., Siraj, L., Collins, J.J., Way, J.C., and Silver, P.A. (2014). Programmable bacteria detect and record an environmental signal in the mammalian gut. Proc. Natl. Acad. Sci. U. S. A. *111*, 4838–4843.

Lambeth, C.R., White, L.J., Johnston, R.E., and de Silva, A.M. (2005). Flow cytometry-based assay for titrating dengue virus. J. Clin. Microbiol. *43*, 3267–3272.

Lanciotti, R.S., Kosoy, O.L., Laven, J.J., Velez, J.O., Lambert, A.J., Johnson, A.J., Stanfield, S.M., and Duffy, M.R. (2008). Genetic and serologic properties of Zika virus associated with an epidemic, Yap State, Micronesia, 2007. Emerg. Infect. Dis. *14*, 1232–1239.

Lu, T.K., Bowers, J., and Koeris, M.S. (2013). Advancing bacteriophage-based microbial diagnostics with synthetic biology. Trends Biotechnol. *31*, 325–327.

de M Campos, R., Cirne-Santos, C., Meira, G.L.S., Santos, L.L.R., de Meneses, M.D., Friedrich, J., Jansen, S., Ribeiro, M.S., da Cruz, I.C., Schmidt-Chanasit, J., et al. (2016). Prolonged detection of Zika virus RNA in urine samples during the ongoing Zika virus epidemic in Brazil. J. Clin. Virol. Off. Publ. Pan Am. Soc. Clin. Virol. *77*, 69–70.

Mlakar, J., Korva, M., Tul, N., Popović, M., Poljšak-Prijatelj, M., Mraz, J., Kolenc, M., Resman Rus, K., Vesnaver Vipotnik, T., Fabjan Vodušek, V., et al. (2016). Zika Virus Associated with Microcephaly. N. Engl. J. Med. *374*, 951–958.

Oehler, E., Watrin, L., Larre, P., Leparc-Goffart, I., Lastere, S., Valour, F., Baudouin, L., Mallet, H., Musso, D., and Ghawche, F. (2014). Zika virus infection complicated by Guillain-Barre syndrome--case report, French Polynesia, December 2013. Euro Surveill. Bull. Eur. Sur Mal. Transm. Eur. Commun. Dis. Bull. *19*.

Pardee, K., Green, A.A., Ferrante, T., Cameron, D.E., DaleyKeyser, A., Yin, P., and Collins, J.J. (2014). Paper-based synthetic gene networks. Cell *159*, 940–954.

Rohrman, B.A., Leautaud, V., Molyneux, E., and Richards-Kortum, R.R. (2012). A lateral flow assay for quantitative detection of amplified HIV-1 RNA. PloS One *7*, e45611.

Schrader, C., Schielke, A., Ellerbroek, L., and Johne, R. (2012). PCR inhibitors - occurrence, properties and removal. J. Appl. Microbiol. *113*, 1014–1026.

Slomovic, S., Pardee, K., and Collins, J.J. (2015). Synthetic biology devices for in vitro and in vivo diagnostics. Proc. Natl. Acad. Sci. U. S. A. *112*, 14429–14435.

Smith, D.W., and Mackenzie, J. (2016). Zika virus and Guillain-Barré syndrome: another viral cause to add to the list. Lancet Lond. Engl.

Stefan, C.P., Chase, K., Coyne, S., Kulesh, D.A., Minogue, T.D., and Koehler, J.W. (2016). Development of real-time reverse transcriptase qPCR assays for the detection of Punta Toro virus and Pichinde virus. Virol. J. *13*, 54.

Tappe, D., Rissland, J., Gabriel, M., Emmerich, P., Gunther, S., Held, G., Smola, S., and Schmidt-Chanasit, J. (2014). First case of laboratory-confirmed Zika virus infection imported into Europe, November 2013. Euro Surveill. Bull. Eur. Sur Mal. Transm. Eur. Commun. Dis. Bull. *19*.

Ulrich, R.M., Casper, E.T., Campbell, L., Richardson, B., Heil, C.A., and Paul, J.H. (2010). Detection and quantification of Karenia mikimotoi using real-time nucleic acid sequence-based amplification with internal control RNA (IC-NASBA). Harmful Algae *9*, 116–122.

Victora, C.G., Schuler-Faccini, L., Matijasevich, A., Ribeiro, E., Pessoa, A., and Barros, F.C. (2016). Microcephaly in Brazil: how to interpret reported numbers? Lancet Lond. Engl. *387*, 621–624.

WHO, (2016). WHO to fast-track availability of diagnostics for Zika virus. Available: http://www.who.int/medicines/news/fast_track_diagnostics_zika/en/.

Yen, C.-W., de Puig, H., Tam, J.O., Gómez-Márquez, J., Bosch, I., Hamad-Schifferli, K., and Gehrke, L. (2015). Multicolored silver nanoparticles for multiplexed disease diagnostics: distinguishing dengue, yellow fever, and Ebola viruses. Lab. Chip *15*, 1638–1641.

Zammarchi, L., Stella, G., Mantella, A., Bartolozzi, D., Tappe, D., Günther, S., Oestereich, L., Cadar, D., Muñoz-Fontela, C., Bartoloni, A., et al. (2015). Zika virus infections imported to Italy: clinical, immunological and virological findings, and public health implications. J. Clin. Virol. Off. Publ. Pan Am. Soc. Clin. Virol. *63*, 32–35.

Zika experimental science team ZIKV-001: Infection of three rhesus macaques with French Polynesian Zika virus. Available: https://zika.labkey.com/project/OConnor/ZIKV-001/begin.view. 2016.

Figure legends

Figure 1. Workflow for the rapid prototyping of paper-based, biomolecular sensors for portable and low-cost diagnostics. Using sequence information from online databases, primers for isothermal RNA amplification and toehold switch-based RNA sensors were designed *in silico* using purpose-built algorithms. Once synthesized, the resulting sequence-specific toehold sensors can be assembled and validated in less than 7 hours. In under a day, validated sensors can be embedded into paper and freeze-dried along with a cell-free transcription and translation system to be deployed in the field as stable diagnostics. For the diagnostic test, extracted RNA is isothermally amplified via NASBA and used to rehydrate the freeze-dried paper sensors. The detection of the appropriate trigger RNA is indicated by a color change in the paper disc from yellow to purple.

Figure 2. Rapid prototyping of 48 paper-based RNA toehold sensors for Zika virus detection. (**A**) Series A toehold switch sensor schematic. The sensor design from Green et al. (2014) was modified with a shortened 11-nt loop sequence to reduce leakage of output gene expression. (**B**) Series B toehold switch sensor schematic. Based on the same Zika genomic region as the A series, these sensors include a 12-nt loop and lack the refolding domain. These modifications were made to further reduce LacZ reporter leakage in the OFF state. (**C**) Maximum fold change in the rate of LacZ production for the Series A Zika virus RNA sensors during the first 90 min at 37°C. Fold change of LacZ production rate is determined from the slope of absorbance at 570 nm over time (sensor alone vs. sensor with 3000 nM RNA trigger). Sensors are ordered according to fold change. (**D**) Maximum fold change in the rate of LacZ production for the Series B Zika virus RNA sensors during the first 90 min at 37°C. Error bars represent SD from three replicates. Inset: average LacZ absorbance of the OFF states at 60 min indicates an overall reduction in LacZ reporter leakage for the Series B sensors. Error bars represent SD across the 24 sensors. See also Figure S1 and Table S1.

Figure 3. Isothermal RNA amplification improves sensitivity of toehold switch sensors to allow for detection of femtomolar concentrations of Zika virus RNA fragments. (**A**) Sensitivity of six of the best performing Series A and B sensors without RNA amplification. Fold change is calculated from absorbance (570 nm) after 30 min at 37°C. Error bars represent SD from three replicates. (**B**) A schematic of NASBA (nucleic acid sequence based amplification)-mediated RNA amplification. (**C**) Zika RNA fragments diluted in water or 7% human serum were amplified using NASBA with input concentrations ranging from 30 pM down to 3 fM. A 1:7 dilution of the NASBA reaction in water was then used to rehydrate freeze-dried, paper-based reactions containing sensors 27B and 32B. Fold change is calculated as described in (A) after 30 min at 37°C. See also Figure S2 and Table S2.

Figure 4. Moving toward a field-ready diagnostic for Zika virus. (**A**) Sequence-specificity of Zika virus sensors 27B and 32B. Sensors were challenged with 3000 nM of RNA corresponding to target sequences from the Zika virus or the homologous region of the Dengue virus. Fold change is calculated from absorbance (570 nm) at 60 min after rehydration and incubation of freeze-dried, paper-based reactions at 37°C. Error bars represent SD from three replicates. (**B**) Zika virus sensors 27B and 32B were tested for specificity using NASBA reaction products derived from 300 fM input RNA corresponding to target genomic regions of the Zika or Dengue viruses in 7% human serum. Fold change was calculated as in (A). (**C**) Using the portable electronic reader, time-course data were collected for Zika virus sensor 32B in the presence of RNA amplified from 1 fM or 3 fM inputs of trigger RNA in 7% human serum. To increase sensitivity, NASBA reactions were run for 2.5 hours. Graphs plot the relative absorbance of 570 nm wavelength light compared to background, which was collected every minute from freeze-dried, cell-free reactions embedded into paper. (**D**) Incorporating viral sample processing into the diagnostic workflow. Lentivirus was packaged with Zika RNA or homologous Dengue RNA fragments targeted by sensor 32B. Three femtomolar of virus was spiked into 7% human serum and heated to 95°C for 2 minutes to extract viral RNA. The boiled lysate was used to initiate NASBA-mediated RNA amplification. A 1:7 dilution of the two-hour NASBA reaction in water was then used to rehydrate freeze-dried paper-based reactions. Time-course data were collected on the portable electronic reader as in (C). See also Figure S3.

Figure 5. NASBA-CRISPR Cleavage (NASBACC) allows for strain differentiation at a single-base resolution. (**A**) Schematic representation of NASBACC genotyping following a positive Zika diagnosis. A synthetic trigger sequence is appended to a NASBA-amplified RNA fragment through reverse transcription. The presence of a strain-specific PAM leads to the production of either truncated or full-length trigger RNA, which differentially activates a toehold switch (sensor H) (Pardee et al., 2014). (**B**) The probability that a non-biased single nucleotide polymorphism (SNP) between two strains can be discriminated by CRISPR/Cas9 is 48% (Table S4). Hence, genetic drift between the American and African or Asian strains, while relatively small (14.4% and 4.9% sequence dissimilarity, respectively), has created hundreds of strain-specific PAM sites. (**C**) A SNP between African (KF268950) and American (KU312312) strains at site 7330 disrupts an existing PAM site, allowing for Cas9-mediated DNA cleavage only in the American strain. (**D**) Sensor 32B can distinguish between Dengue and Zika RNA sequences, but cannot discriminate between American and African Zika strains. Paper discs containing sensor 32B were rehydrated with 300 nM trigger RNA corresponding to sequences from American-Zika, African-Zika, or Dengue. Colorimetric outputs: a purple color indicates the activation of LacZ expression from the toehold switch, and a yellow color indicates the toehold switch remained inactive. (**E**) NASBACC can discriminate between American- and African-lineages of Zika virus. Paper discs containing sensor H were rehydrated with a 1:10 dilution of NASBACC reactions initiated with 0.05 µl of a 300 nM RNA sample. In this case, an inactive toehold switch leads to a positive identification of the American Zika strain.

Figure 6. Validation of diagnostic workflow on live Zika virus samples. (**A**) Specificity of sensor 32B against purified genomic RNA. Sensor 32B was tested for specificity using NASBA reaction products performed on 30 fM RNA purified from Zika virus and three different Dengue virus serotypes. Fold change is calculated from absorbance (570 nm) at 60 min after rehydration and incubation of freeze-dried, paper-based reactions at 37°C. Error bars represent SD from three replicates. (**B**) Detection of live Zika virus. Ten femtomolar of laboratory-cultured Zika virus was spiked into human serum (7%), heated to 95°C for 2 minutes, and used to initiate NASBA-mediated RNA amplification. A 1:7 dilution of the three-hour NASBA reaction in water was then used to rehydrate freeze-dried, paper-based reactions. Time-course data were collected on the portable electronic reader. Graph plots the relative absorbance of 570 nm wavelength light compared to background. Error bars represent SD from three replicates. (**C, D**) Detection of Zika virus in viremic rhesus macaque plasma using sensors 27B and 32B. Plasma containing 2.8 fM of Zika virus was diluted 1:10 in nuclease free water, heated to 95°C for 2 minutes, and used to initiate NASBA-mediated RNA amplification. Three-hour NASBA reactions were monitored on the portable electronic reader as in (B).

Figure1

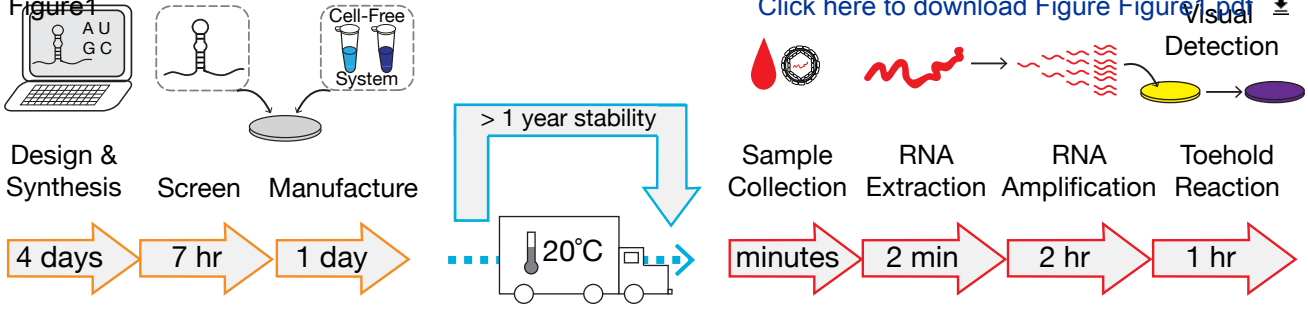

Figure2

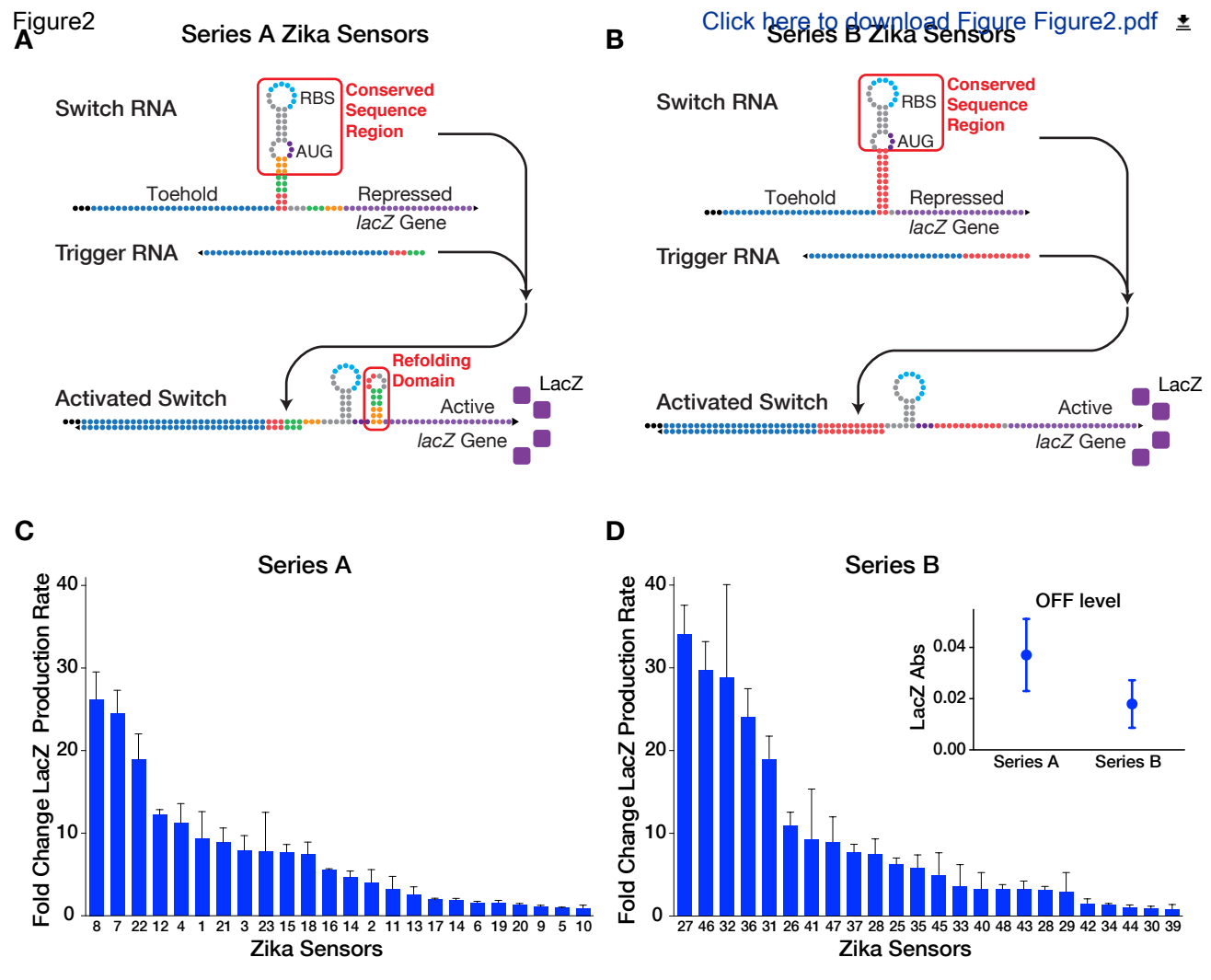

Figure3

Click here to download Figure Figure3.pdf

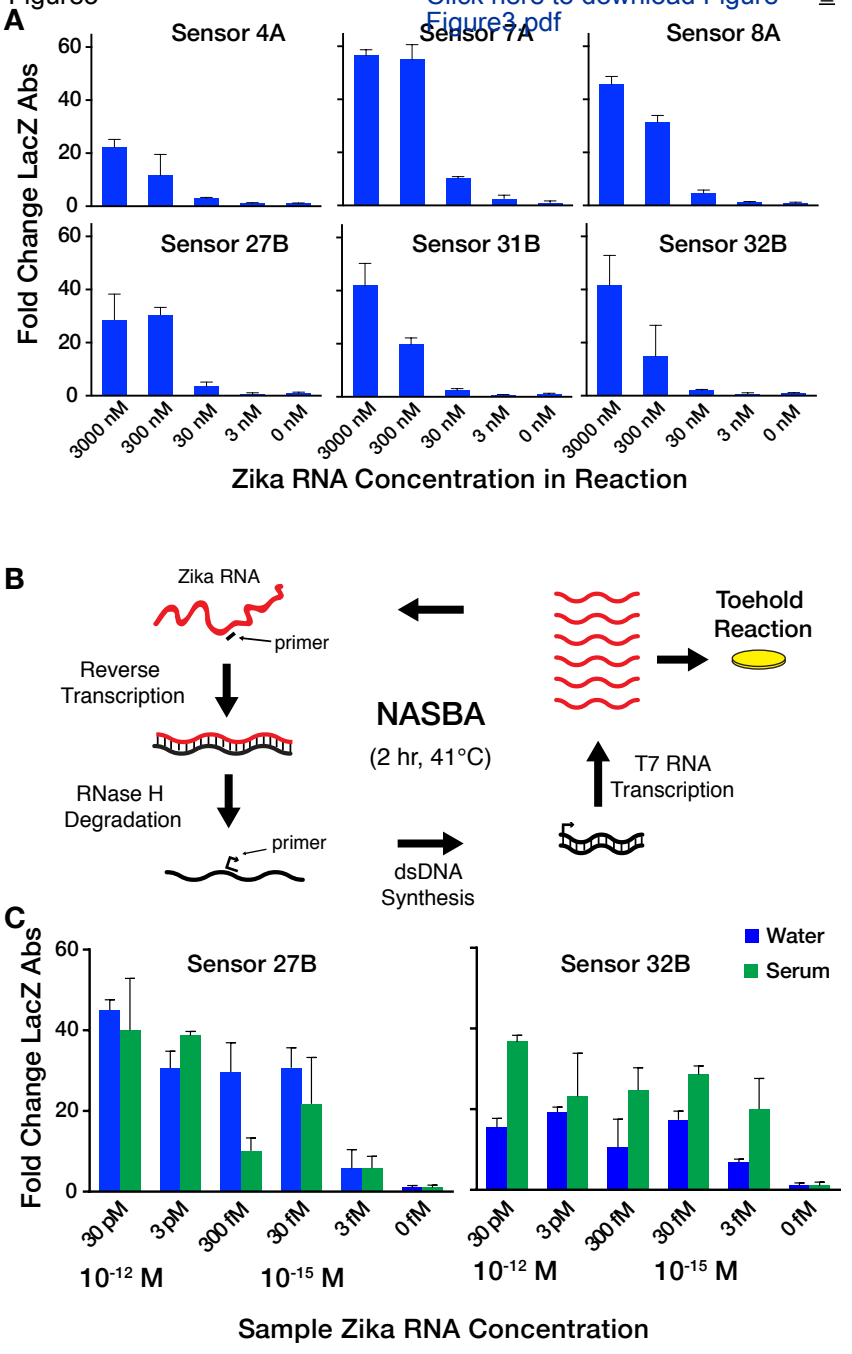

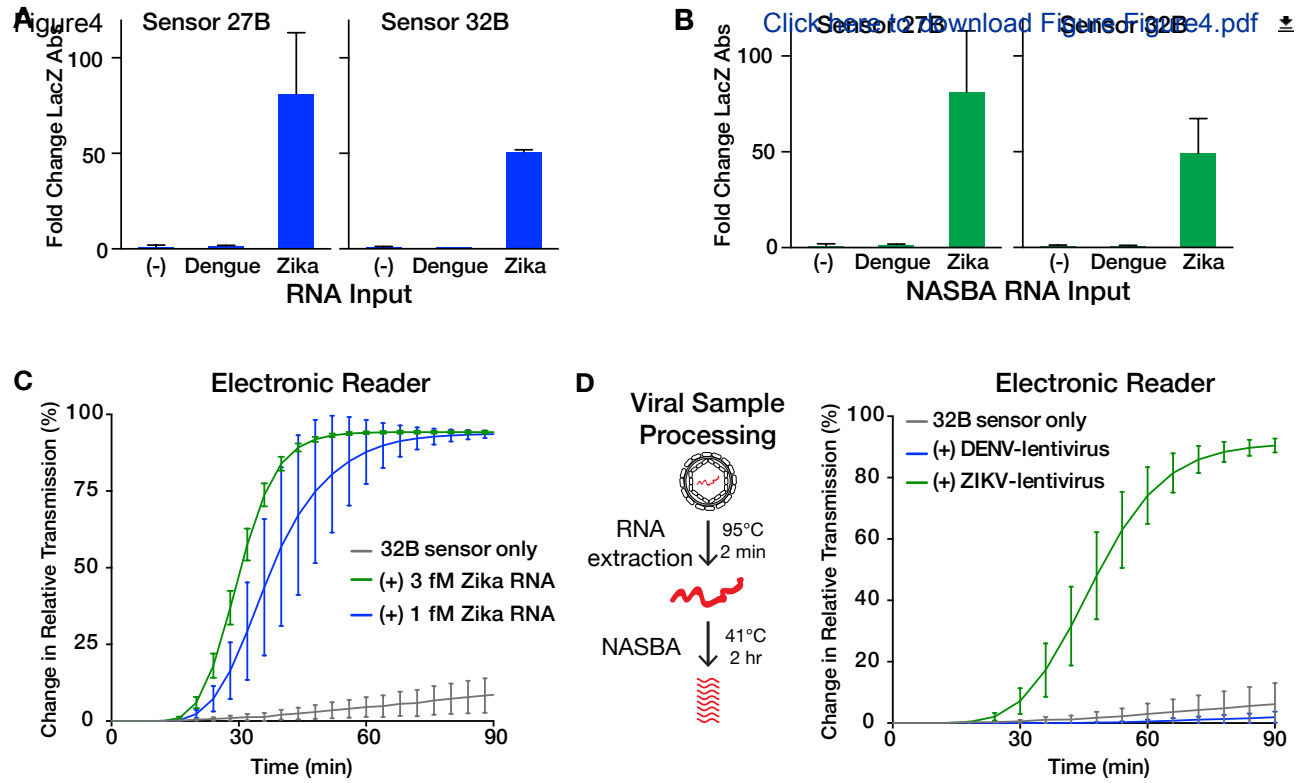

Figure5

Click here to download Figure Figure5.pdf

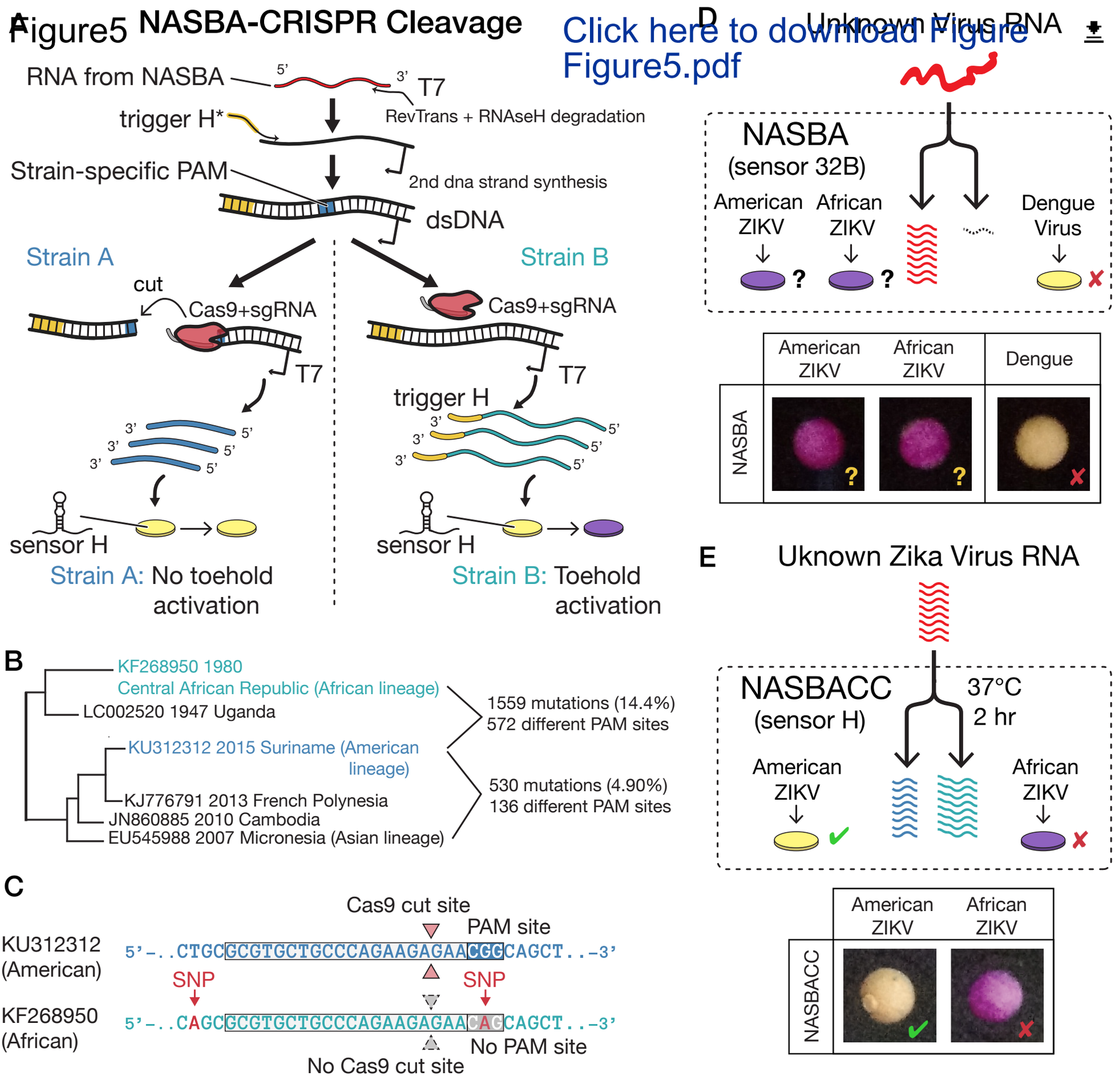

Figure6

Click here to download Figure Figure6.pdf

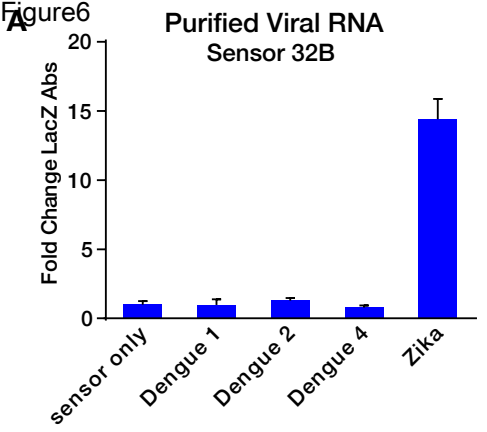

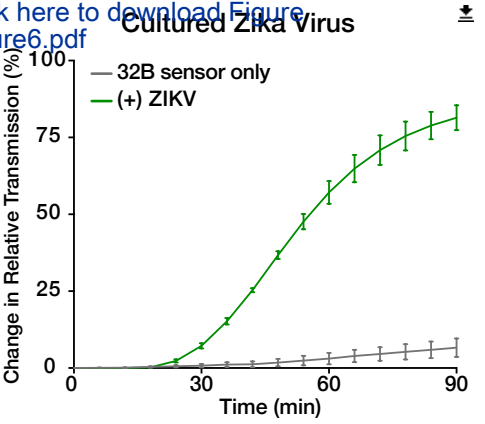

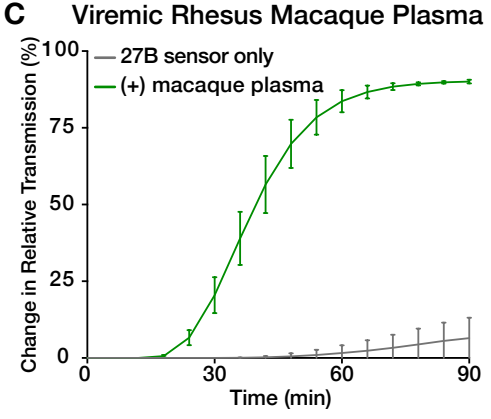

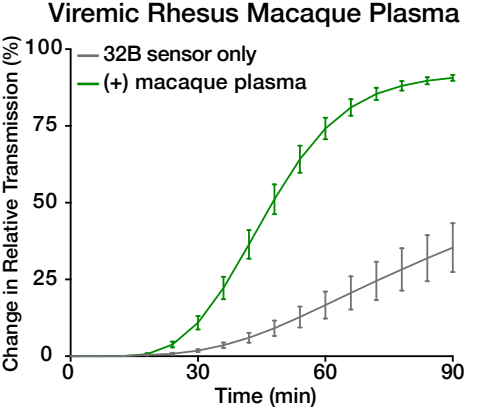

Extended description for the supplemental information:

In Silico Strategy for Toehold Switch Sensor and NASBA Primer Design

We developed an integrated *in silico* strategy for generating optimal NASBA primers and toehold switches for detection of Zika. Mirroring the procedure used for running the paper-based diagnostic assay, we initially generated a set of optimal primers for the NASBA reaction and then developed a series of toehold switch designs screened for activity on the RNA transcripts produced by NASBA.

Identification of Optimal NASBA Primers for Zika Amplification

We generated a set of potential primer pairs with favorable characteristics for NASBA reactions as described by Deiman et al. (Deiman et al., 2002). Specifically, we analyzed the Zika genome to identify all potential forward and reverse priming sites that had the following characteristics:

1. GC content between 40-60%
2. Template hybridization regions of 20- to 24-nts and with DNA melting temperatures above 41°C
3. No consecutive runs of four or more nucleotides
4. An A base at the final 3' nucleotide
5. Minimal DNA primer internal secondary structure, including the T7 promoter region
6. Minimal DNA primer dimer formation probability
7. Higher GC content in the 6-nts at the 5' end of the primer that hybridized to the template
8. Higher AT content in the 6-nts at the 3' end of the primer

All subsequences from the Zika genome that did not satisfy requirements 1 to 4 were immediately eliminated from consideration. The remaining primers were then analyzed for characteristics 5-8 and the deviation from optimal 50% GC content, with each parameter converted into a numerical score. The forward NASBA primers, which append the T7 promoter site to NASBA DNA intermediate, were modeled with this T7 promoter site present. Accordingly, the prefix sequence AATTCTAATACGACTCACTATAGGGAGAAGG (T7 promoter sequence underlined) was appended to the 5' end of each forward primer. The resulting scores were combined and used to estimate the overall favorability of every potential primer in the Zika genome. Following this initial screen, the top 2% of all the potential primers were then compared to the rest of the Zika genome to determine the longest contiguous region of the primer that matched more than one site in the genome. This comparison provided a coarse check of primer specificity in advance of more detailed primer specificity screening conducted later in the design process. The length of this contiguous region for each primer was then incorporated into a final score for each primer.

The first stage of screening resulted in a set of forward and reverse primers to provide optimal characteristics for binding to the target genome; however, it did not consider other important effects on NASBA efficiency, namely the length and secondary structure of the amplicon produced by NASBA. To consider these amplicon-related effects, we first identified the binding sites for each primer on the genome and, if more than one primer acted at the same site, and selected the primer awarded the highest favorability score. We then constructed a set of potential forward and reverse primer pairs based on the recommended amplicon lengths for successful NASBA reactions. Although NASBA is known to work best with amplicons having lengths between approximately 120-nts to 250-nts (Deiman et al., 2002), our rapid screening approach initially employs synthetic DNA strands as templates for transcribing the target RNA. Since the length of these DNA oligos (IDT Ultramers) is currently limited to 200-nts including the T7 promoter site, we instead examined primer pairs for amplicons ranging from 120- to 176-nts in length. After applying all the above constraints on primer and amplicon sequences, we were left with a set of 4351 potential NASBA primer pairs. The RNA amplicons generated for each of these primers pairs were then assessed for their secondary structure. NASBA reactions are known to be more effective when applied to templates having low secondary structure. Consequently, we examined the degree of amplicon single-strandedness using the NUPACK ensemble defect function (Zadeh et al., 2011a, 2011b).

Next, each of the potential NASBA primers were then coarsely screened for sequence similarities with 11 viruses known to be closely related to Zika: Dengue virus 1, Dengue virus 2, Dengue virus 3, Dengue virus 4, West Nile virus, St. Louis encephalitis virus, yellow fever virus, Powassan virus, Semliki Forest virus, O'nyong'nyong virus, and Chikungunya virus. Sequence similarities were estimated by determining the maximum contiguous sequence in the primer that was found in any of the 11 related viruses. More stringent specificity screening was carried out in later stages as described below.

After all the above screening procedures, the final NASBA primer pairs were sorted by quality after taking into account the favorability scores of each primer, the secondary structure of the amplicon, and the potential for non-specific binding with other viruses.

Identification of Optimal Toehold Switches for NASBA Products
Out of the 4351 NASBA amplicons, we selected the top 1025 as potential targets for toehold switches. The *in silico* design process for these toehold switches followed closely that previously used for designing mRNA sensors *in vivo* (Green et al., 2014) and on paper (Pardee et al., 2014). Briefly, we designed toehold switch mRNA sensors that hybridized to the NASBA amplicon at 1-nt increments. This sliding window encompassed the internal region of the NASBA product outside of the primer binding sites. This internal region was selected to avoid any potential for sensor activation or competitive binding by residual NASBA primers. The resulting toehold switches were analyzed for secondary structure and toehold availability, and screened to eliminate any sensors with unwanted in-frame stop codons in the output gene sequence. The target transcript itself was again assayed for single-strandedness and availability of the sensor binding sites. The above factors were incorporated into a sensor design score as described previously (Green et al., 2014). The highest scoring toehold switch sensor for each amplicon was then passed on to the final selection stage.

Final Design Selection Process
After the above screening and design stages, we assembled the set of 1025 NASBA primer pairs with corresponding optimized toehold switch sensors. The top overall designs were selected by combining the favorability scores obtained from the NASBA and toehold switch evaluation steps. The primer and sensor sequences from these top designs were then tested for specificity against the human transcriptome and the same panel of closely related viral genomes listed above using NCBI/Primer-BLAST. Moreover, they were screened for specificity within the Zika genome itself. Ultimately, the top 24 designs that survived the Primer-BLAST specificity stage were selected for testing using our rapid *in vitro* screening approach.

Modifying the Toehold Switch Sensor Design for Decreased Signal Leakage
Detailed studies of the toehold switch design parameters (Green et al., 2014) and thermodynamic considerations suggested two simple strategies for decreasing leakage from the toehold switches: reducing the size of the loop containing the ribosome binding site (RBS) in the sensor, and further stabilization of the sensor stem. We applied both these strategies in the Zika-specific toehold switches.

We have previously found that the ON and OFF state signals from the toehold switches increase as the size of the loop in the switch RNA increases. This effect is likely due to two factors: increased accessibility of the RBS to the ribosome, which promotes translation in the presence or absence of the target RNA; and entropic effects that discourage stem formation as the loop becomes longer. Conversely, decreasing the size of the loop is associated with lower leakage, albeit with a decrease in ON state activity. Stabilizing the switch RNA stem by adding additional base pairs or by eliminating the downstream refolding domain (Green et al., 2014) increases the free energy required to unwind the sensor stem and thus encourages decreased signal leakage.

In accordance with above factors, we tested two different types of toehold switches aiming to lower leakage. The first type of sensor, referred to as the A series, are nearly identical to those previously used for mRNA sensing (Green et al., 2014; Pardee et al., 2014), except their loop domain has been reduced from 18-nts to 11-nts. These A sensors retained the downstream refolding domain to encourage sensor triggering and they all have the same sequence at the top of the sensor stem-loop (GUUAUAGUUAUGAACAGAGGAGACAUAACAUGAAC) as illustrated in Figure 2A.

The second type of sensor, referred to as the B series, possesses a stem that has been lengthened by one base pair overall and a loop region that is only 12-nts. Importantly, the B sensors also lack the downstream refolding domain to further stabilize the OFF state. The parental toehold switch for the B sensors exhibited extremely low leakage in preliminary measurements in paper-based reactions and provided a sizeable ON/OFF ratio of ~600-fold regulating GFP expression in *E. coli*. These B sensors all featured the same conserved sequence (GGACUUUAGAACAGAGGAGAUAAAGAUG) at the top of their stem-loops as illustrated in Figure 2B.

Considerations of Sequence Information in Design of the Biomolecular Diagnostics

Evolutionary drift
At the time we began our experiments, few complete genomes for the Zika virus had been reported. In fact, the first complete genome of the strain circulating in the Americas was only published on January 7 in The Lancet (Enfissi et al., 2016). However, previous comparisons of Zika strains do provide information on the degree of evolutionary drift for the virus. Haddow et al. found that a Zika strain isolated in Malaysia in 1966 differed by only 4.3% in nucleotide sequence from isolates obtained Micronesia and Cambodia in 2007 and 2010, respectively (Haddow et al., 2012). Authors also found ≤11.7% nucleotide sequence difference between African and Asian virus lineages, which they argued provided sufficient conserved sequence for genetic tests for both lineages. More recent studies have shown the rate of mutation of Zika is ~10^{-3} nucleotide changes/site/year, which is relatively high among flaviviruses, but a manageable rate for our diagnostic assay (Faria et al., 2016).

Specificity of the NASBA/toehold switch isothermal assay
Since our experiments are performed at mostly 41°C and 37°C, melting-temperature-dependent tuning of primer specificity is not possible in our assays. The benefit of this temperature limitation is that our NASBA and toehold switch detection schemes are able to tolerate mismatches and compensate for variability in the sequence of the target RNA molecules. We have analyzed the binding between the toehold switch 32B, our highest performing sensor, and RNAs from homologous regions in Zika strains isolated from Africa (Uganda, Nigeria, Senegal) and Asia (Malaysia, Cambodia, French Polynesia). All these strains are predicted to fully activate the toehold sensors even with up to 4-nt (11%) mismatches.

Compensating for evolutionary drift
The above analysis is borne out in data showing that sensor 32B can detect the target sequence from both the American and African strains of the virus (Figure 5E). This flexibility in sequence detection is balanced with the three combined layers of specificity in our biomolecular approach. This includes the extensive *in silico* screening of NASBA primers and toehold switch sequences to limit cross-reactivity with off-target sequences and the single-base discrimination of NASBACC. The net result is a programmable platform that can be manufactured to produce diagnostics with both high sequence specificity and the capacity to manage sequence diversity as pathogens evolve. It is also worth mentioning that, in addition to increasing specificity, NASBACC can be used to remove non-specific sequences from samples as well as aid in the discovery mutations in the target regions.

Integration with signature erosion analysis tools

In the future, we plan to integrate existing tools for identifying optimal primer sites for sequence-specific detection into our toehold switch/NASBA primer design algorithms. Software such as BioVelocity (Sozhamannan et al., 2015) and TOPSI (Vijaya Satya et al., 2010) are adept at determining conserved sequence regions across multiple genomes and eliminating those shared with other pathogens or humans. Using these valuable tools, we can rapidly generate a set of specific sites for NASBA priming and toehold switch binding. We can then subject these carefully selected regions to the same screening by toehold secondary structure and NASBA primer characteristics described in this work.

Freeze-dried NASBA
For freeze-dried NASBA experiments, Enzyme Mix was lyophilized separately from the other components. The solution containing reaction buffer, nucleotide mix, RNase inhibitor, and primers was reconstituted in 15% DMSO, while the Enzyme Mix was reconstituted in nuclease-free water. Once reconstituted, the experiments proceeded as described in the Experimental Procedures section.

Freeze-dried CRISPR/Cas9 nuclease assay
Reactions were performed in a 30 µl volume of 1x Cas9 Nuclease Reaction Buffer (NEB #M0386S) containing 30 nM of guide RNA (gRNA), 30nM of Cas9 Nuclease (*S. pyogenes*, NEB #M0386S), and 3 nM of substrate DNA (pAG_TS1_KS001 plasmid). Six gRNA sequences targeting the lacZ gene (Doench et al., 2014) inserted into plasmid pAG_TS1_KS001 were used for the CRISPR/Cas9 freeze-dried assay (Figure S5A). All components except substrate DNA were first combined in a 27 µl reaction volume and incubated for 10 minutes at 25°C to allow Cas9+gRNA to form duplexes. For fresh reactions, 3 µl of a 30 nM solution of substrate DNA was added to the solution. For freeze-dried reactions, the 27 µl solution was lyophilized overnight and reconstituted with 30 µl of a solution containing 3 nM of substrate DNA. After the addition of substrate DNA, the solution was incubated for 1 h at 37°C and run on a 1% agarose gel for fragment analysis (Figure S5B).

Care and use of macaques at the Wisconsin National Primate Research Center
All Indian-origin rhesus macaque monkeys from which plasma was isolated were cared for by the staff at the Wisconsin National Primate Research Center (WNPRC) in accordance with the regulations and guidelines outlined in the Animal Welfare Act and the Guide for the Care and Use of Laboratory Animals and the recommendations of the Weatherall report. This study was approved by the University of Wisconsin-Madison Graduate School Institutional Animal Care and Use Committee (Animal Care and Use Protocol Number G005401). For all procedures (i.e., physical examination, virus inoculation, blood and swab collection), animals were anesthetized with an intramuscular dose of ketamine (10 ml/kg). Blood samples were obtained using a vacutainer system or needle and syringe from the femoral or saphenous vein.

Zika virus stock production for macaque infection
ZIKV strain H/PF/2013 (GenBank accession number: KJ776791), originally isolated from a 51-year-old female in France returning from French Polynesia with a single round of amplification on Vero cells, was obtained from Xavier de Lamballerie (European Virus Archive, Marseille France). Virus stocks were prepared by inoculation onto a confluent monolayer of C6/36 mosquito cells. A single harvest of virus with a titer of 1.26×10^6 PFU/ml for the Asian-lineage (equivalent to 1.43×10^9 vRNA copies/ml) was used.

Zika virus challenge of macaques, plasma collection and processing
The virus stock was thawed, diluted in PBS to the appropriate concentration for each challenge, and loaded into a 1 ml syringe that was kept on ice until challenge. Animals were anesthetized as described above, and 1 ml of inocula was administered subcutaneously over the cranial dorsum. At the conclusion of the procedure, animals were closely monitored by veterinary and animal care staff for adverse reactions and signs of disease. Fresh plasma and PBMC were isolated from EDTA-treated whole blood by Ficoll

density centrifugation at 1860 rcf for 30 min. The plasma layer was collected and centrifuged for an additional 8 min at 670 rcf to remove residual cells. The supernatant plasma was then filtered over a 0.45 µm syringe filter. Collected plasma was diluted 1:10 in nuclease free water. Diluted samples were heated to 95°C for two minutes and immediately added to a NASBA reaction as described above. NASBA was run for three hours.

References:

Deiman, B., van Aarle, P., and Sillekens, P. (2002). Characteristics and applications of nucleic acid sequence-based amplification (NASBA). Mol. Biotechnol. *20*, 163–179.

Doench, J.G., Hartenian, E., Graham, D.B., Tothova, Z., Hegde, M., Smith, I., Sullender, M., Ebert, B.L., Xavier, R.J., and Root, D.E. (2014). Rational design of highly active sgRNAs for CRISPR-Cas9-mediated gene inactivation. Nat. Biotechnol. *32*, 1262–1267.

Enfissi, A., Codrington, J., Roosblad, J., Kazanji, M., and Rousset, D. (2016). Zika virus genome from the Americas. Lancet Lond. Engl. *387*, 227–228.

Faria, N.R., Azevedo, R. do S. da S., Kraemer, M.U.G., Souza, R., Cunha, M.S., Hill, S.C., Thézé, J., Bonsall, M.B., Bowden, T.A., Rissanen, I., et al. (2016). Zika virus in the Americas: Early epidemiological and genetic findings. Science.

Green, A.A., Silver, P.A., Collins, J.J., and Yin, P. (2014). Toehold switches: de-novo-designed regulators of gene expression. Cell *159*, 925–939.

Haddow, A.D., Schuh, A.J., Yasuda, C.Y., Kasper, M.R., Heang, V., Huy, R., Guzman, H., Tesh, R.B., and Weaver, S.C. (2012). Genetic characterization of Zika virus strains: geographic expansion of the Asian lineage. PLoS Negl. Trop. Dis. *6*, e1477.

Pardee, K., Green, A.A., Ferrante, T., Cameron, D.E., DaleyKeyser, A., Yin, P., and Collins, J.J. (2014). Paper-based synthetic gene networks. Cell *159*, 940–954.

Sozhamannan, S., Holland, M.Y., Hall, A.T., Negrón, D.A., Ivancich, M., Koehler, J.W., Minogue, T.D., Campbell, C.E., Berger, W.J., Christopher, G.W., et al. (2015). Evaluation of Signature Erosion in Ebola Virus Due to Genomic Drift and Its Impact on the Performance of Diagnostic Assays. Viruses *7*, 3130–3154.

Vijaya Satya, R., Kumar, K., Zavaljevski, N., and Reifman, J. (2010). A high-throughput pipeline for the design of real-time PCR signatures. BMC Bioinformatics *11*, 340.

Zadeh, J.N., Steenberg, C.D., Bois, J.S., Wolfe, B.R., Pierce, M.B., Khan, A.R., Dirks, R.M., and Pierce, N.A. (2011a). NUPACK: Analysis and design of nucleic acid systems. J. Comput. Chem. *32*, 170–173.

Zadeh, J.N., Wolfe, B.R., and Pierce, N.A. (2011b). Nucleic acid sequence design via efficient ensemble defect optimization. J. Comput. Chem. *32*, 439–452.

Figure S1. Results of Zika virus sensor screening (Related to Figure 2). Using low-volume paper-based reactions +/- 3000 nM RNA (36 nt) corresponding to the targeted Zika virus genomic RNA sequence of each sensor. Data represent absorbance at 570 nm plotted over time.

Figure S2. Sensor specificity and sensitivity (Related to Figure 3). (A) Linear response of sensors 27B, 31B and 32B to corresponding RNA trigger at 0 nM, 3 nM, 30 nM and 300 nM. Each point represents the mean of triplicate data taken at 60 min. (B) Orthogonality of sensors 27B, 7A and 32B to treatments of 3000 nM of trigger RNA from each of the three sensors. The absorbance output (570 nm) of the sensors at each time point was converted to a ratio of the maximum absorbance of respective sensor at the 90-min time point and plotted as a heat map. Yellow indicates no sensor activation and purple indicates maximum sensor activation. (C) Reproducibility of NASBA reactions. Samples of Zika RNA in water or 7% human serum were amplified in three independent 2-hour NASBA reactions. Each NASBA reaction was diluted 1:7 in water and used to rehydrate three freeze-dried, paper-based reactions containing sensor 27B for a total of nine replicates. Fold change was calculated from absorbance (570 nm) after 30 min at 37°C. Error bars represent SD from nine replicates for the 3 pM sample and three replicates for the 0 pM sample. (D) Effect of NASBA reaction time on sensitivity. Samples of Zika RNA in 7% human serum were amplified in NASBA reactions for 30, 60, and 90 min. Diluted NASBA reactions (1:7) were tested with sensor 32B. Fold change was calculated as above. Error bars represent SD of three replicates. (E) NASBA with freeze-dried reagents. Samples of Zika RNA in 7% human serum were amplified by NASBA reagents in the standard formulation and by reagents freeze-dried in-house. Fold change and error bars were calculated as above after 60 min. (F) Removing the 65°C step from NASBA protocol. Samples of Zika RNA in 7% human serum incubated at 95°C for two minutes, mimicking viral lysis, and then amplified by NASBA according to the standard procedure without the 65°C step. Fold change and error bars were calculated as above after 60 min.

Figure S3. Sequence alignments and RNA extraction optimization (Related to Figure 4). Sequence alignments of Zika virus and Dengue virus genomic regions targeted by sensors (A) 27B and (B) 32B. Red boxes indicates sequences targeted by the respective toehold switches, red and blue boxes indicate the NASBA-amplified regions, and the remaining sequence indicates natural flanking RNA sequences from each virus. The entire Zika 32 sequence shown here was cloned into lentivirus to make proxy Zika virus. (C) Effect of boiling time on RNA extraction. Lentivirus was packaged with the Zika virus RNA fragment corresponding to sensor 32B. Virus was diluted to 10 and 3 fM target RNA in 7% human serum. Twenty-five µL of virus was heated to 95°C for 1 and 2 minutes. One µL was then used to initiate NASBA-mediated RNA amplification. A 1:7 dilution of 2 hour NASBA reactions in water was then used to rehydrate freeze-dried, paper-based reactions. Fold change was calculated from absorbance (570 nm) after 60 min at 37°C. Error bars represent SD of three replicates.

Figure S4. Portable electronic optical reader (Related to Figure 4). (A) Line drawings used to cut the housing for the electronic reader from black acrylic using a laser cutter. (B) Image of the 16-reaction reader from the front. Chip containing paper-based sensors slides into the slot illuminated by the green light. Reader dimensions: 106 mm wide x 116 mm deep x 96 mm high. (C) Components and circuit design used to assemble the electronic optical reader.

Figure S5. CRISPR nuclease assay using fresh and freeze-dried reactions (Related to Figure 5). (A) Sequence information and location of the gRNA used to target the LacZ gene. Each sequence was selected for maximum activity using the Doench et al. scoring algorithm (Doench et al., 2014) (B) Gel showing the length of supercoiled vs. cut DNA following the *in vitro* digestion of a LacZ-containing plasmid for fresh and freeze-dried reactions. Note that the activity of some gRNA/Cas9 combinations is improved under freeze-dried conditions.

Table S1. Sequences of Toehold Switch Sensors and Corresponding Target Sequences in Zika Genome (related to Figure 2 and Figure S1).

Table S2. Sequences of NASBA Primers Used for Zika RNA Amplication (related to Figure 3 and Figure S2).

Table S3. Portable electronic reader build of materials (related to Figure 4 and Figure S4).

Table S4. Probabilities of PAM site disruption from single point mutations (Related to Figure 5 and Figure S5).

Table S1. Sequences of Toehold Switch Sensors and Corresponding Targ

NOTES:

1. The sequence GGG was added to the 5' end of all sensor RNA and target RNA fragment sequ
2. The GGG prefix is not shown in the sensor sequences in the table so that the target RNA bind
3. The coding sequence of the reporter protein lacZ was added immediately after the switch RNA
4. Two Zika virus strains (KU312312, AY632535) have sufficient sequence homology to be detec
5. Target RNAs fragments for sensors 7A/31B and 11A/35B have a GGGAGAAGG sequence ad
6. Target RNA fragments for sensors 12A/36B have a GGGAGAAG sequence added at the 5' er

Target sequence in Zika virus genome	Location in genome	Sensor Name
UUGAGAGUGAGAAGAAUGACACAUGGAGGCUGAAGA	3027	1A
AUGAUGGGAAAAAGAGAAAAGAAACAAGGGGAAUUU	8963	2A
GACACAGGACAUGAAACUGAUGAGAAUAGAGCGAAA	1373	3A
UGGAAAACAUCAUGUGGAGAUCAGUAGAAGGGGAGC	2610	4A
GGGGAAAAAAGAGGCUAUGGAAAUAAUAAAGAAGUU	256	5A
GAUAACGCCCAAUUCACCAAGAGCCGAAGCCACCCU	1414	6A
UUGAAGAGGAAAAAGAGUGGAAGACUGCAGUGGAAG	8841	7A
UUUUGCUCGUGGCGCACUACAUGUACUUGAUCCCAG	7188	8A
UUGCUACUCACAAUUAACACCCCUGACCCUAAUAGU	7144	9A
ACCACCUCAUACAACAACUACUCCUUAAUGGCGAUG	7022	10A
ACCACAAAGAUCAUCAUAAGCACAUCAAUGGCAGUG	3563	11A
AGACAGAGUUCCAGAAAACAAAACAUCAAGAGUGGG	5721	12A
UGCACAAUGCCCCCACUGUCGUUCCGGGCUAAAGAU	3368	13A
GACACCGGAACUCCACACUGGAACAACAAAGAAGCA	1598	14A
GUUUGCCGCUGGGAAAAGAGGAGCGGCUUUUGGAGU	6379	15A
GGCAGAAGUGUGGACCAGACACGGAGAGAAAAGAGU	6277	16A
CUGAUCGAGAUGAAAACAUGUGAAUGGCCAAAGUCC	3071	17A
GAGCCAGAAAAGCAAAGAUCUCCCCAGGACAACCAA	6761	18A
CUUAACACAUUUACCAACCUAGUGGUGCAACUCAUU	9431	19A
GCGGUACAGGGGUGUUCGUCUAUAACGACGUUGAAG	2466	20A
GAGGCUGAGGAAGUUCUAGAGAUGCAAGACUUGUGG	9476	21A
GGCACAGUGAAGAGCUUGAAAUUCGGUUUGAGGAAU	3225	22A
CAUCUAAUGGGAAGGAGAGAGGAGGGGGCAACCAUA	6890	23A
GAUAGGUUUGCACAUGCCCUCAGGUUCUUGAAUGAU	9620	24A

Zika virus from the Americas genome sequence (Accession number: KU312312; 10,374-nts)	ACAGGUUUUAUUUUGGAU UCAUGAAAAACCCAAAAAA UUGUCAAUAUGCUAAAACC CCCUUUGGGGGCUUGAAG GCUGGGUCAUGGGCCCAU UAGCCUUUUUGAGAUUCA GUCUCAUCAAUAGAUGGG GCUAUGGAAAUAAUAAAGA GCCAUGCUGAGAAUAAUC AGACGAGGCGCAGAUACU CCUGCUGACCACAGCUAU GUGGGAGUGCAUACUAUA CUGGGGAGGCCAUAUCUU

MR 766 Zika virus genome, Uganda 1947 (Accession number: AY632535; 10,794-nts)	AGUUGUUGAUCUGUGUGA GUCUGAAGCGAGAGCUAA UUUGGAUUUGGAAACGAG CCAAAGAAGAAAUCCGGAC UAAAACGCGGAGUAGCCC UUGAAGAGGUUGCCAGCC ACCCAUCAGAAUGGUUUU AUUUACAGCAAUCAAGCCA AUGGGGUUCCGUGGGGAA AAAGAAGUUCAAGAAAGAU AAUCAAUGCUAGGAAAGAC CACCAGCAUCGGAAUCAUU

et Sequences in Zika Genome (related to Figure 2 and Figure S1)

uences for efficient expression by T7 RNA polymerase. If the RNA sequence began with G or G
ling site can be readily identified.
A sequences in the tables.
cted using the same toehold switch sensors (27B, 32B).
dded at the 5' end.
nd.

A Series Sensors	B Series Sensors	
Sensor sequence	**Sensor Name**	**Sensor sequence**
UCUUCAGCCUCCAUGUGUCAU	25B	UCUUCAGCCUCCAUGUGUCAUUCUUC
AAAUUCCCCUUGUUUCUUUUC	26B	AAAUUCCCCUUGUUUCUUUUCUCUUU
UUUCGCUCUAUUCUCAUCAGU	27B	UUUCGCUCUAUUCUCAUCAGUUUCAU
GCUCCCCUUCUACUGAUCUCC	28B	GCUCCCCUUCUACUGAUCUCCACAUG
AACUUCUUUAUUAUUUCCAUA	29B	AACUUCUUUAUUAUUUCCAUAGCCUCU
AGGGUGGCUUCGGCUCUUGG	30B	AGGGUGGCUUCGGCUCUUGGUGAAU
CUUCCACUGCAGUCUUCCACU	31B	CUUCCACUGCAGUCUUCCACUCUUUU
CUGGGAUCAAGUACAUGUAGU	32B	CUGGGAUCAAGUACAUGUAGUGCGCC
ACUAUUAGGGUCAGGGGUGUU	33B	ACUAUUAGGGUCAGGGGUGUUAAUUG
CAUCGCCAUUAAGGAGUAGUU	34B	CAUCGCCAUUAAGGAGUAGUUGUUGU
CACUGCCAUUGAUGUGCUUAU	35B	CACUGCCAUUGAUGUGCUUAUGAUGA
CCCACUCUUGAUGUUUUGUUU	36B	CCCACUCUUGAUGUUUUGUUUUCUGG
AUCUUUAGCCCGGAACGACAG	37B	AUCUUUAGCCCGGAACGACAGUGGGG
UGCUUCUUUGUUGUUCCAGUG	38B	UGCUUCUUUGUUGUUCCAGUGUGGAG
ACUCCAAAAGCCGCUCCUCUU	39B	ACUCCAAAAGCCGCUCCUCUUUUCCCA
ACUCUUUUCUCUCCGUGUCUG	40B	ACUCUUUUCUCUCCGUGUCUGGUCCA
GGACUUUGGCCAUUCACAUGU	41B	GGACUUUGGCCAUUCACAUGUUUUCA
UUGGUUGUCCUGGGGAGAUCU	42B	UUGGUUGUCCUGGGGAGAUCUUUGCU
AAUGAGUUGCACCACUAGGUU	43B	AAUGAGUUGCACCACUAGGUUGGUAA
CUUCAACGUCGUUAUAGACGA	44B	CUUCAACGUCGUUAUAGACGAACACC
CCACAAGUCUUGCAUCUCUAG	45B	CCACAAGUCUUGCAUCUCUAGAACUU
AUUCCUCAAACCGAAUUUCAA	46B	AUUCCUCAAACCGAAUUUCAAGCUCU
UAUGGUUGCCCCCUCCUCUCU	47B	UAUGGUUGCCCCCUCCUCUCUCCUUC
AUCAUUCAAGAACCUGAGGGC	48B	AUCAUUCAAGAACCUGAGGGCAUGUG

UUGGAAACGAGAGUUUCUGG
GAAAUCCGGAGGAUUCCGGA
GCGGAGUAGCCCGUGUGAGC
AGGCUGCCAGCCGGACUUCU
JCAGGAUGGUCUUGGCGAUUC
CGGCAAUCAAGCCAUCACUGG
GUUCAGUGGGGAAAAAAGAG
AAGUUCAAGAAAGAUCUGGCU
AAUGCUAGGAAGGAGAAGAAG
AGUGUCGGAAUUGUUGGCCU
GGCAGCGGAGGUCACUAGAC
UGUACUUGGACAGAAACGAUG
UUCCAACCACAUUGGGGAUG


AGUCAGACUGCGACAGUUCGA
CAACAGUAUCAACAGGUUUAA
AGUUUCUGGUCAUGAAAAACC
GGAUCCGGAUUGUCAAUAUGC
GUGUAAACCCCUUGGGAGGU
GGACUUCUGCUGGGUCAUGG
GGCGAUACUAGCCUUUUUGAG
AUCACUGGGCCUUAUCAACAG
AAAAAGAGGCUAUGGAAAUAAU
JCUUGCUGCCAUGUUGAGAAU
GAGGAAGAGACGUGGCGCAGA
JGGCCUCCUGCUGACUACAGC

ɜG, only GG or G, respectively, was added to the 5' end of the sequence.

Target RNA Fragment Used for Initial Sensor Screening			
Sequence	**Genome Start site**	**Genome End site**	**Genome fragment length**
GGGCAGUGAUCUAGGCUACUGGA	3007	3170	164
GGGUGCCAGAGUUGUGUGUACAA	8941	9098	158
GGGCCAGCACAGUGGGAUGAUCG	1348	1494	147
GGGCGGGAUCUCCUCUGUUUCAA	2586	2733	148
GGGCCAUCACUGGGUCUCAUCAA	220	385	166
GGGAAUGCUGUCAGUUCAUGGCU	1327	1494	168
GGGAGAAGGAUGGUCUCUUCCUG	8729	8920	192
GGGCUGACCCUAAUAGUGGCCAU	7166	7299	134
GGGUUUGGUAUGGGCAAAGGGAU	7078	7228	151
GGGCCAUCUAUGCUGCCUUGACA	6966	7141	176
GGGAGAAGGGUGAUUCUGCUCAU	3521	3702	182
GGGAGAAGGGUUUGUUCCAAGCG	5628	5850	223
GGGAGAUCAACCACUGCAAGCGG	3316	3445	130
GGGAGUGGUUCCACGACAUUCCA	1555	1711	157
GGGUGGACGCCAGAGUUUGUUCA	6330	6458	129
GGGCUGCCGGAAUAACCUACACA	6198	6351	154
GGGCUACUGGAUUGAGAGUGAGA	3017	3170	154
GGGCAGCCAGAAUUGCAUGUGUC	6702	6874	173
GGGAGCGGACAAGUUGUCACUUA	9404	9581	178
GGGUGCUCGGUGGACUUCUCAAA	2429	2578	150
GGGAGUGGUGCAACUCAUUCGGA	9451	9584	134
GGGCAAUACCAGAGAGGGCUACA	3184	3334	151
GGGAGUAGGUCUUCUGGGCUUGA	6820	6952	133
GGGAUAGGCUCAAACGAAUGGCA	9561	9688	128

Table S2. Sequences of NASBA Primers Used for Zika RNA Amplication (related to Fi

NOTES:

1. NASBA experiments on the MR 766 Zika virus were only conducted using NASBA primers for sensor 32B.

Toehold Switch Sensor		NASBA Primers for Zika Virus from the Americas (KU312312)	
A Series	**B series**	**Forward**	**Reverse**
1A	25B	AATTCTAATACGACTCACTATAGGGA	GCCCAGCTAAAGACTTGGGTATGA
2A	26B	AATTCTAATACGACTCACTATAGGGA	CATCCAGTGATCCTCGTTCA
3A	27B	AATTCTAATACGACTCACTATAGGGA	CCTGTCCTCGGTTCACAATCAA
4A	28B	AATTCTAATACGACTCACTATAGGGA	AATCTCTGTGGACCTCTCCA
5A	29B	AATTCTAATACGACTCACTATAGGGA	GAGGCCAACAATTCCGACACTA
6A	30B	AATTCTAATACGACTCACTATAGGGA	CTGTCCTCGGTTCACAATCA
7A	31B	AATTCTAATACGACTCACTATAGGGA	CCAGAACCTTGGATCGTTCA
8A	32B	AATTCTAATACGACTCACTATAGGGA	CCATCCACAACAGGGTTCTTCA
9A	33B	AATTCTAATACGACTCACTATAGGGA	CAGCCCTGGGATCAAGTACATGTA
10A	34B	AATTCTAATACGACTCACTATAGGGA	GCCCATACCAAACAACACTCCA
11A	35B	AATTCTAATACGACTCACTATAGGGA	GCTTAGCCAGGTCACTCATTGA
12A	36B	AATTCTAATACGACTCACTATAGGGA	AAGTTGGCGCCCATCTCTGAAA
13A	37B	AATTCTAATACGACTCACTATAGGGA	GTTCTTTCCTGGGCCTTATCTCCA
14A	38B	AATTCTAATACGACTCACTATAGGGA	CCTTCTTGACTCCCTAGAACCA
15A	39B	AATTCTAATACGACTCACTATAGGGA	ATCTCTCTGTCATGTGTCCTGGCA
16A	40B	AATTCTAATACGACTCACTATAGGGA	TCTGAACAAACTCTGGCGTCCA
17A	41B	AATTCTAATACGACTCACTATAGGGA	GCCCAGCTAAAGACTTGGGTATGA
18A	42B	AATTCTAATACGACTCACTATAGGGA	TGTTCTCTCCAACCATCCGA
19A	43B	AATTCTAATACGACTCACTATAGGGA	GCTCTGCAACCAGTTAGTCA
20A	44B	AATTCTAATACGACTCACTATAGGGA	ATCTTCCCAGGCTTGCTTGA
21A	45B	AATTCTAATACGACTCACTATAGGGA	TGCCATTCGTTTGAGCCTATCCCA
22A	46B	AATTCTAATACGACTCACTATAGGGA	GCAGTGGTTGATCTCAGAGA
23A	47B	AATTCTAATACGACTCACTATAGGGA	CGCAGGTCAATGTCCATTGAGA
24A	48B	AATTCTAATACGACTCACTATAGGGA	CCACTCTTGTGTGTCCTTCCTA

gure 3 and Figure S2)

NASBA Primers for MR 766 Zika Virus (AY632535)	
Forward	**Reverse**
AATTCTAATACGACTCACTATAGG(	CCTGTCCTCGGTTCACAATCAA
AATTCTAATACGACTCACTATAGG(	CCATCCACAACGGGATTCTTCA

Table S3. Portable electronic reader build of materials (related to Figure 4 and F

		total $:	244.238		
Vendor	**quantity**	**price**	**total price**	**item #**	**description**
Adafruit	1	24.95	24.95	50	Arduino Uno R3 (Atmega328 -
Adafruit	1	19.95	19.95	2078	Adafruit PowerBoost 500 Shiel
Adafruit	1	12.5	12.5	2011	Lithium Ion Battery - 3.7v 2000
Adafruit	1	19.95	19.95	1141	Adafruit Assembled Data Logg
Adafruit	1	7.95	7.95	102	SD/MicroSD Memory Card (4 (
Adafruit	16	6.26	100.16	1980	Adafruit TSL2591 High Dynam
Sparkfun	3	2.8	8.4	PRT-12702	SparkFun Solder-able Breadbo
Digi-Key	2	0.49	0.98	A19473-ND	CONN HEADER VERT 9POS
Digi-Key	2	0.643	1.286	A19476-ND	CONN HEADER VERT 13POS
Digi-Key	2	1.21	2.42	A31001-ND	CONN RECEPT 9POS 28AW(
Digi-Key	2	1.93	3.86	A30954-ND	CONN RECEPT 13POS 28AW
Digi-Key	20	0.2246	4.492	36-621-ND	BRACKET RT ANG MOUNT 4
McMaster-Carr	1	2.36	2.36	90760A005	Zinc Plated Steel Narrow Hex
McMaster-Carr	1	6.74	6.74	8505K11	Black Acrylic, for reader
McMaster-Carr	2	8.04	16.08	92095A453	M2 screws, for attaching sensc
McMaster-Carr	1	1.04	1.04	90592A004	M2 nuts, for attaching sensors
Inventables	1	4.84	4.84	23876-35	Clear acrylic, for bottom half of
Inventables	1	6.28	6.28	24112-04	Black acrylic, for top half of cas

Figure S4)

- assembled)
ld - Rechargeable 5V Power Shield
)mAh
ging shield for Arduino
GB SDHC)
iic Range Digital Light Sensor

oard - Mini

.100 TIN
S .100 TIN
G MTA100
VG MTA100
4-40 STEEL, for reader assembly

Nut 4-40 Thread Size, 3/16" Wide, 1/16" High, for reader assembly

ors

f cassette
ssette

pwr	pwr
gnd	gnd
s0	s0
s1	
	s1
s2	
s3	s2
data	s3
clock	LED

Table S4. Probabilities of PAM site disruption from single point mutations (Related to Figure 5 and Figure S5).

A. Summary of the effect of single point mutations

12 PAM sites
4 double PAM sites
32 PAM site created
12 double PAM site created
32 PAM site destroyed
12 double PAM site destroyed
4 PAM site inverted

Each mutation has a 23% probability (**44/192**) of creating a new PAM site, a 23% probability (**44/192**) of destroying and existing PAM site, and a 2% probability (**4/192**) of inverting the orientation of an existing PAM site.

Overall, any given point mutations has a 48% probability (**92/192**) of disrupting an existing PAM site.

B. Detailed list of all single point mutations on every 3-bp sequences.

Center letter: A								
Last→ First ↓	A		C		G		T	
A	AAA	ACA	AAC	**ACC**	AAG	ACG	AAT	ACT
		AGA		AGC		**AGG**		AGT
		ATA		ATC		ATG		ATT
C	CAA	**CCA**	CAC	**CCC**	CAG	**CCG**	CAT	**CCT**
		CGA		CGC		**CGG**		CGT
		CTA		CTC		CTG		CTT
G	GAA	GCA	GAC	**GCC**	GAG	GCG	GAT	GCT
		GGA		**GGC**		**GGG**		**GGT**
		GTA		GTC		GTG		GTT
T	TAA	TCA	TAC	**TCC**	TAG	TCG	TAT	TCT
		TGA		TGC		**TGG**		TGT
		TTA		TTC		TTG		TTT

Center letter: C								
Last→ First ↓	A		C		G		T	
A	ACA	ACA	**ACC**	**AAC**	ACG	AAG	ACT	AAT
		AGA		**AGC**		**AGG**		AGT
		ATA		**ATC**		ATG		ATT
C	**CCA**	**CAA**	**CCC**	**CAC**	**CCG**	**CAG**	**CCT**	**CAT**
		CGA		**CGC**		**CGG**		**CGT**
		CTA		**CTC**		**CTG**		**CTT**
G	GCA	GAA	**GCC**	**GAC**	GCG	GAG	GCT	GAT
		GGA		**GGC**		**GGG**		**GGT**
		GTA		**GTC**		GTG		GTT
T	TCA	TAA	**TCC**	**TAC**	TCG	TAG	TCT	TAT
		TGA		**TGC**		**TGG**		TGT
		TTA		**TTC**		TTG		TTT

Center letter: G								
Last→ First ↓	A		C		G		T	
A	AGA	AAA	AGC	**ACC**	**AGG**	**AAG**	AGT	AAT
		ACA				**ACG**		ACT
		ATA		ATC		**ATG**		ATT
C	CGA	CAA	CGC	**CCC**	**CGG**	**CAG**	CGT	CAT
		CCA				**CCG**		**CCT**
		CTA		CTC		**CTG**		CTT
G	**GGA**	**GAA**	**GGC**	**GAC**	**GGG**	**GAG**	**GGT**	**GAT**
		GCA		GCC		**GCG**		**GCT**
		GTA		**GTC**		**GTG**		**GTT**
T	TGA	TAA	TGC	**TCC**	**TGG**	**TAG**	TGT	TAT
		TCA				**TCG**		TCT
		TTA		TTC		**TTG**		TTT

Center letter: T								
Last→ First ↓	A		C		G		T	
A	ATA	AAA	ATC	**ACC**	ATG	AAG	ATT	AAT
		ACA				**ACG**		ACT
		AGA		AGC		**AGG**		AGT
C	CTA	CAA	CTC	**CCC**	CTG	**CAG**	CTT	**CAT**
		CCA				**CCG**		**CCT**
		CGA		CGC		**CGG**		CGT
G	GTA	GAA	GTC	**GAC**	GTG	GAG	GTT	GAT
		GCA		**GCC**		GCG		GCT
		GGA		**GGC**		**GGG**		**GGT**
T	TTA	TAA	TTC	**TAC**	TTG	TAG	TTT	TAT
		TCA		**TCC**		**TCG**		TCT
		TGA		TGC		**TGG**		TGT

Table S1

12 PAM sites
4 double PAM sites
32 PAM site creations
12 double PAM site creations
32 PAM site destructions
12 double PAM site destructions
4 PAM site inversions
All 64 3-gram sequences create 20 PAM sites. A single point mutation will change the 3-gram's middle base. Each mutation has a 23% probability (**44/192**) of creating a new PAM site, a 23% probability (**44/192**) of destroying and existing PAM site, and a 2% probability (**4/192**) of inverting the orientation of an existing PAM site. Overall, any given point mutations has a 48% probability (**92/192**) of disrupting an existing PAM site.

Supplemental Figure S1

Click here to download Supplemental Figure FigureS1.pdf

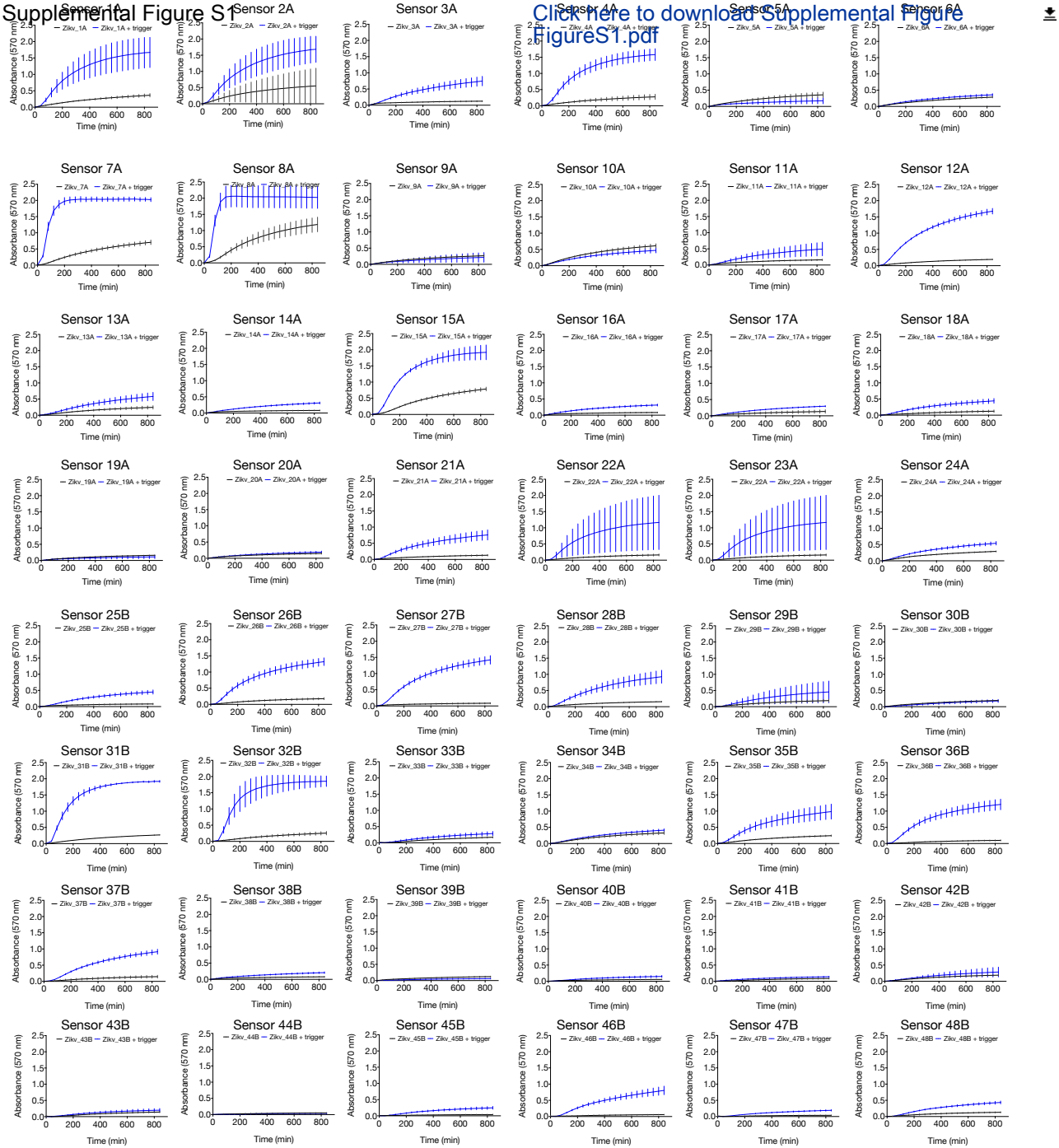

Supplemental Figure S2

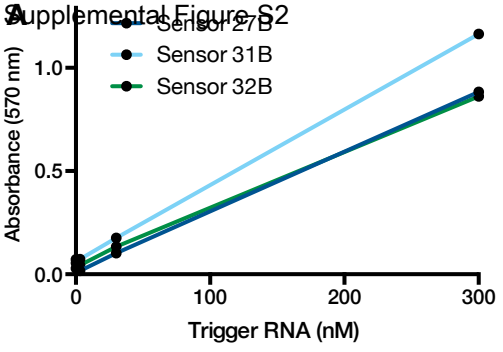

B Click here to download Supplemental Figure FigureS2.pdf

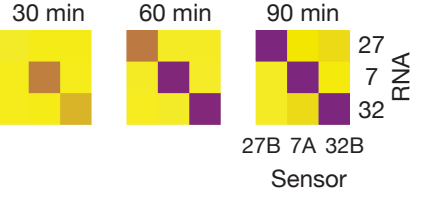

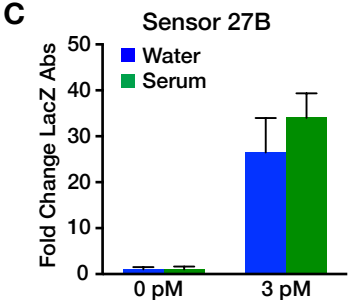

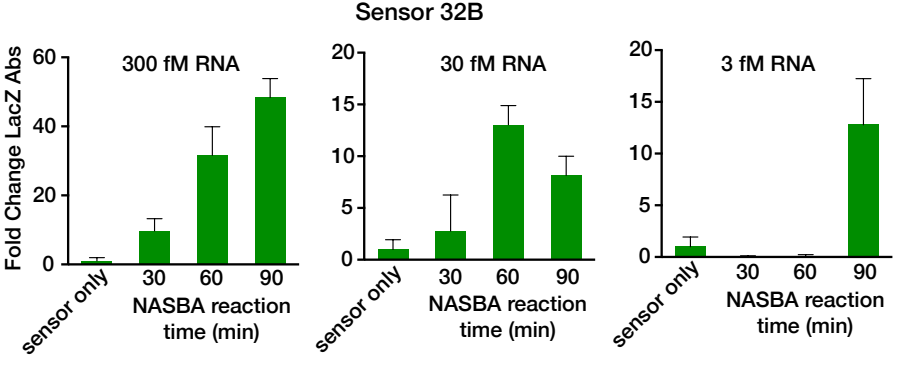

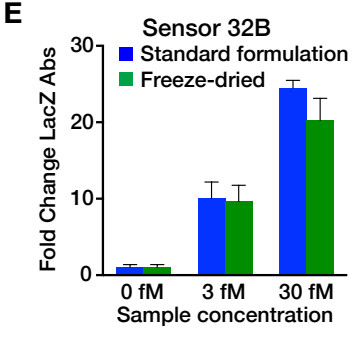

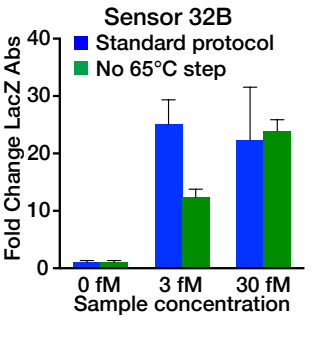

Supplemental Figure S3

Click here to download Supplemental Figure

A

```
Zika27    1   TTGTGCACATGCGCTAAGTTT CTATGCCCCA AGAAAATGAC CGGCAAGAGC
Dengue27  1   TATTGACGTG TGCCAAGTTC AAGTGTGTGA CAAAACTAGA AGGAAAGATA

Zika27    51  ATCCAGCCAG AGAATCTGGA GTACCGGATA ATGCTGTCAG TTCA- - - TGG
Dengue27  51  GTTCAATATG AAAACCTAAA ATATTCAGTG ATAGTCACTG TCCACACTGG

Zika27    101 CTCCCAGCAC AGTGGGATGA TCGTTAATGA CACAGGACAT GAAACTGATG
Dengue27  101 GGACCAGCAC CAGGTGGGAA ACGAGACT- - -ACAGAACAT GGAACAATTG

Zika27    151 AGAATAGAGC GAAAGTTGAG ATAACGCCCA ATTCACCAAG AGCCGAAGCC
Dengue27  151 CGAC - - - - - C - - - A - - - - - - - -TAACACCTC AAGCTCCCAC GTCGGAAATA

Zika27    201 ACCCTGGGGG GGTTTGGAAG CCTAGGACTT GATTGTGAAC CGAGGACAGG
Dengue27  201 CAGCTGACCG ACTACGGAGC CCTCACATTG GACTGCTCAC CTAGAACAGG

Zika27    251 CCTTGACTTT TCAGATTTGT ATTACTTGAC TATGAATAAC AAGCACTGGC
Dengue27  251

Zika27    301 TGGTTCACAA GGAGTGGTTC CACGACATTC CATTACCTTG GCACGCTGGG
Dengue27  301
```

B

```
Zika32    1   AGCTGGAGTG TTGTTTGGTA TGGGCAAAGG GATGCCATTC TACGCATGGG
Dengue32  1   GGCAGCTATAT TGATGGGAC TTGACAAGGG ATGGCCAATA TCGAAGATGG

Zika32    51  ACTTTGGAGT CCCGCTGCTA ATGATAGGTT GCTACTCACA ATTAACACCC
Dengue32  51  ACATAGGAGT TCCACTTCTC GCCTTAGGGT GCTATTCCCA GGTGAACCCA

Zika32    101 CTGACCCTAA TAGTGGCCAT CATTTTGCTC GTGGCGCACT ACATG- TACT
Dengue32  101 TTGACACTGA CAGCGGCGGT GTTGATGTTA GTGGCTCATT ATGCCATAAT

Zika32    151 TGATCCCAGG GCTGCAGGCA GCAGCTGCGC GTGCTGCCCA GAAGAGAACG
Dengue32  151 TGGACC- AGG ACTGCAAGCA AAGGCCACTA GAGAAGCTCA AAAAAGGACA

Zika32    201 GCAGCTGGCA TCATGAAGAA CCCTGTTGTG GATGGAATAG TGGTGACTGA
Dengue32  201 GCGGCCGGAA TAATGAAAAA TCCAACCGTA GACGGGATTG TTGCAATAGA

Zika32    251 CATTGACACA ATGACAATTG ACCCCCAAGT GGAGAAAAAG ATGGGACAGG
Dengue32  251 CTTGGATCCT GTGGTTTATG ATACAAAATT TGAAAAACAG CTAGGCCAAA

Zika32    301 - - - TGCTACT CATAGCAGTA GCCGTCTCCA GCGCCATA  338
Dengue32  301 TAATGTTACT GATA- CTTTG  TACATCAC- A  GATCCTC-  338
```

C

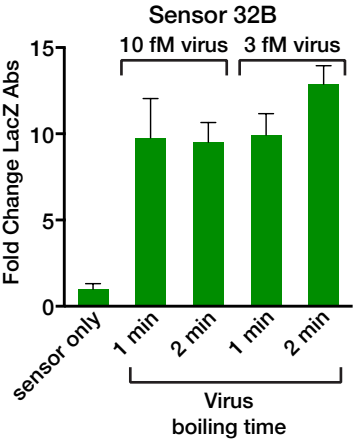

Supplemental Figure S4

Click here to download Supplemental Figure FigureS4.pdf

A

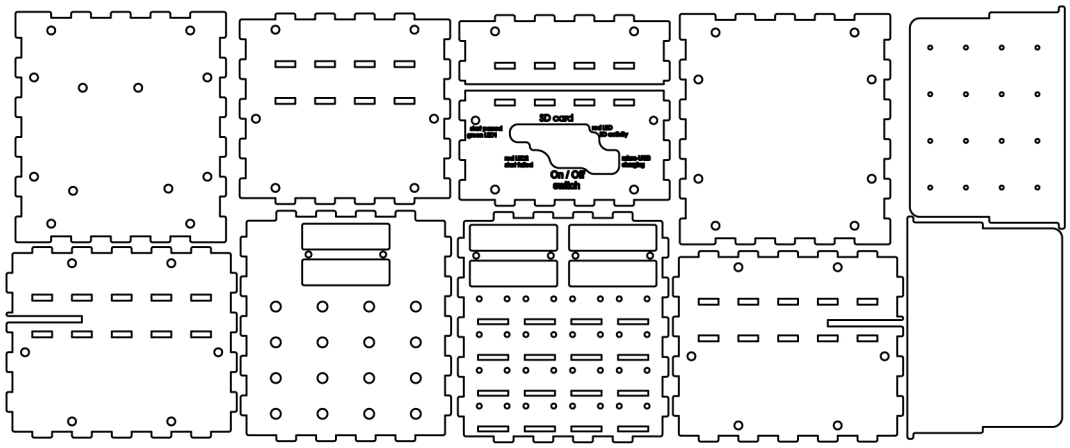

B

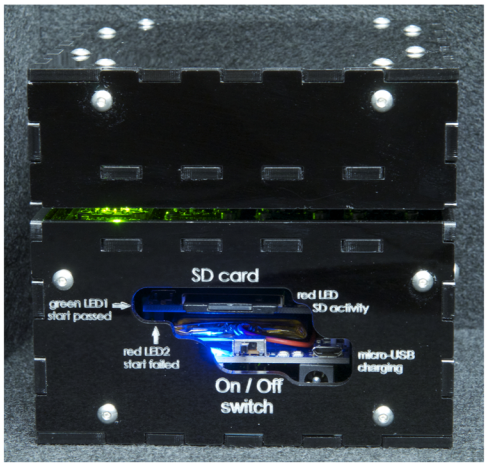

C

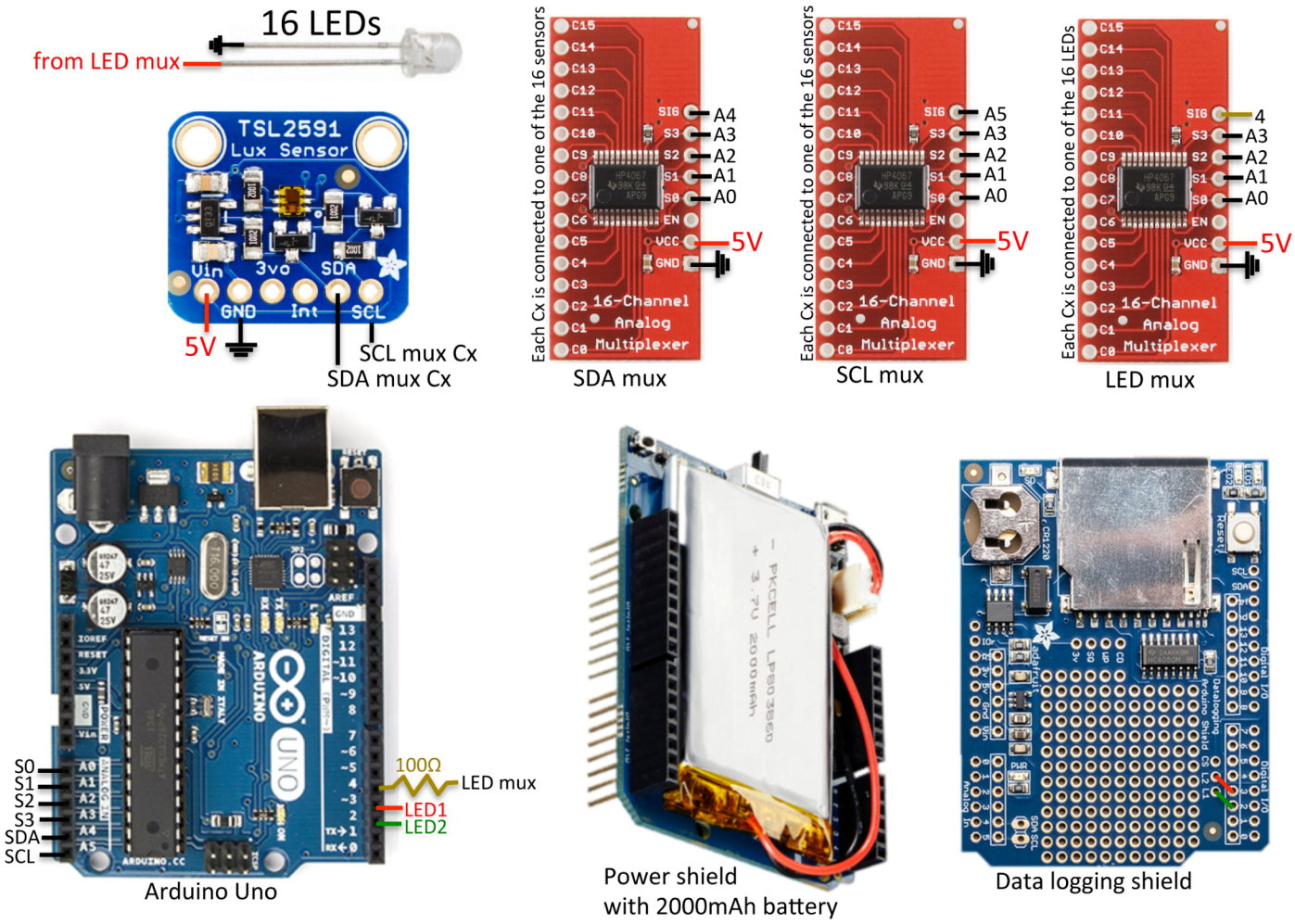

A Supplemental Figure S5

Click here to download Supplemental Figure FigureS5.pdf

	CRISPR target sequence + PAM site	LacZ Position	DNA Strand	Doench et. al score
gRNA-1	cttcagcctccagtacagcg**cgg**	717	antisense	86.6
gRNA-2	gttcccacggagaatccgac**ggg**	360	sense	90.9
gRNA-3	ctgcgatgtcggtttccgcg**agg**	1001	sense	88.6
gRNA-4	tggaagatcaggatatgtgg**cgg**	610	sense	80.0
gRNA-5	ttaacgcctcgaatcagcaa**cgg**	1051	antisense	88.4
gRNA-6	gcgcgtcgtgattagcgccg**tgg**	1398	antisense	86.8

B

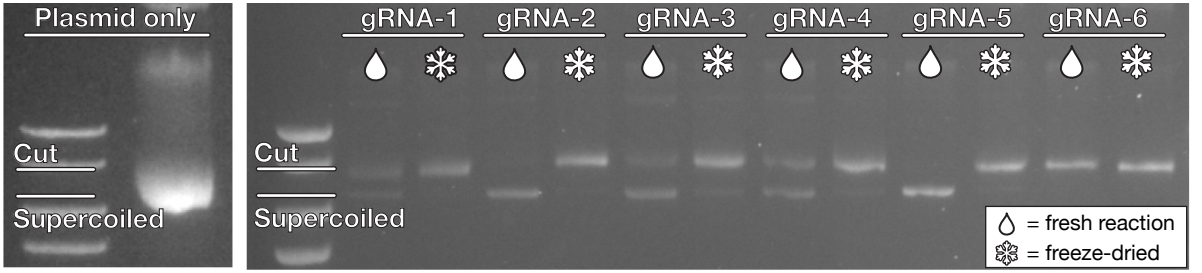

Data analysis and reader code

Click here to access/download

ZIP File

Code.zip